5642 *Biochemistry* **2009,** *48,* 5642–5657
DOI: 10.1021/bi900272r

BIOCHEMISTRY
including biophysical chemistry & molecular biology
Article

Antimicrobial Action of Prototypic Amphipathic Cationic Decapeptides and Their Branched Dimers†

Pooja C. Dewan,‡ Aparna Anantharaman, Virander S. Chauhan, and Dinkar Sahal*

Malaria Research Laboratory, International Centre for Genetic Engineering and Biotechnology, Aruna Asaf Ali Marg, New Delhi 110067, India ‡Present address: Molecular Biophysics Unit, Indian Institute of Science, Bangalore 560012, India

Received May 5, 2008; Revised Manuscript Received May 8, 2009

ABSTRACT: Toward delineation of antimicrobial action, a prototypic amphipathic, cationic decapeptide Ac-G-**X**-R-K-**X**-H-K-**X**-W-A-NH_2 was designed and peptides for which **X** was didehydrophenylalanine (ΔFm), α-aminoisobutyric acid (Um), or phenylalanine (Fm) were synthesized. A growth kinetics experiment indicated that the bacteriostatic effects were nil (Um), mild and transient (Fm), and strong and persistent (ΔFm) respectively. Though at par in binding to lipopolysaccharide, ΔFm and Fm, but not Um, caused outer membrane permeabilization. Inner membrane permeabilization was attenuated and membrane architecture rehabilitated with ΔFm but not Fm. Reverse phase high-performance liquid chromatography revealed that ΔFm was translocated into *Escherichia coli*, while Um and fragments of Fm were detected in the medium. Among these monomers, only ΔFm was modestly antibiotic [minimum inhibitory concentrations (MICs) of 110 μM (*E. coli*) and 450 μM (*Staphylococcus aureus*)]. Interestingly, a linear dimer of ΔFm, viz. $(\Delta Fm)_2$, turned out to be highly potent against *E. coli* [MIC of 2 μM and minimum bactericidal concentration (MBC) of 2 μM] and modestly potent against *S. aureus* (MIC of 20 μM and MBC of 20 μM). In contrast, a lysine-based branched dimer of ΔFm, viz. ΔFd, was found to be a potent antimicrobial against both *E. coli* (MIC of 2.5 μM) and *S. aureus* (MIC of 5 μM). Studies with analogous branched dimers of Fm and Um have indicated that dimerization represents a scaffold for potentiation of antimicrobial peptides and that the presence of ΔF confers potent activity against both *E. coli* and *S. aureus*. De novo design has identified ΔFd as a potent, noncytotoxic, bacterial cell-permeabilizing and -penetrating antimicrobial peptide, more protease resistant than its monomeric counterpart. We report that in comparison to the subdued and sequential "membrane followed by cell interior" mode of action of the monomeric ΔFm, the strong and simultaneous "membrane along with cell interior" targeting by the dimeric ΔFd potentiates and broadens its antibiotic action across the Gram-negative−Gram-positive divide.

The arrival of antibiotics was one of the greatest milestones in human and animal health. Today, however, the advent of antibiotic resistance to virtually every known class of natural and synthetic compounds (*1*, *2*) represents a serious problem in clinical medicine. This calls for an urgent need to discover newer designs of antibiotics with novel mechanisms of action. Species across the evolutionary tree produce a large repertoire of antibiotic peptides (*3*), sequences of several hundred of which are now in the database http://www.bbcm.univ.trieste.it/~tossi/antimic.html. However, for reasons of low potency, toxicity, high cost, or short half-life (*4*), Nature's peptide antibiotics have not found much use in clinical practice. Different approaches are being used to counter these problems which include preparation of analogues of naturally existing antimicrobial peptides (AMPs)[1] (*5*), screening of combinatorial libraries (*6*), and de novo design of AMPs (*7*). However, a thorough understanding of the mode of action of AMPs is a prerequisite for the rational design of novel AMPs. Various structure−activity relationship studies on AMPs (*8*) and evasion strategies developed by resistant

†This research was funded through a grant (BT/PR3325/BRB/10/283/2002) to D.S. from the Department of Biotechnology, Government of India. Research fellowships of the Council of Scientific and Industrial Research, Government of India, to P.C.D. and A.A. are acknowledged.

*To whom correspondence should be addressed. Phone: 91-11-2674 1358. Fax: 91-11-2616 2316. E-mail: dinkar@icgeb.res.in.

[1]Abbreviations: AMPs, antimicrobial peptides; ATCC, American type Culture Collection; CFU, colony forming units; FACS, fluorescence-activated cell sorting; FITC, fluorescein isothiocyanate; Fmoc, fluorenyl methoxy carbonyl; LPS, lipopolysaccharide; MBC, minimum bactericidal concentration; MIC, minimum inhibitory concentration; PXB, polymyxin B; RPHPLC, reverse phase high-performance liquid chromatography; SEM, scanning electron microscopy; TEM, transmission electron microscopy; Fm, ΔFm, and Um, monomeric peptides with phenylalanine (F), didehydrophenylalanine (ΔF), and α-aminoisobutyric acid (U), respectively, in the **X** positions of the peptide sequence Ac-G-**X**-R-K-**X**-H-K-**X**-W-A-NH_2; Fd, ΔFd, and Ud, branched dimeric peptides with phenylalanine (F), didehydrophenylalanine (ΔF), and α-aminoisobutyric acid (U), respectively, at the **X** positions of the corresponding dimeric peptide sequences; D-Lys-ΔFd, nonhelical dimeric analogue of ΔFd in which lysines 4 and 7 are in the D configuration.

 Published on Web 05/11/2009

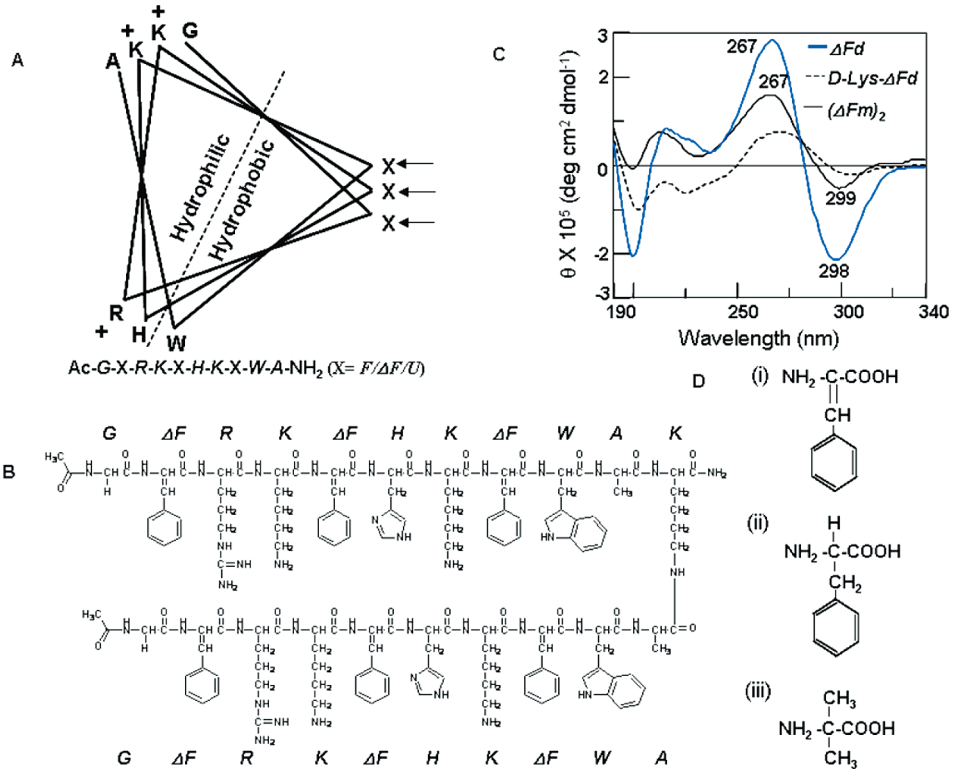

FIGURE 1: De novo design of antimicrobial peptides. (A) Prototypic amphipathic cationic decapeptide sequence in a 3_{10}-helical wheel configuration where arrows mark the apolar X residues and plus signs denote cationic residues. (B) ChemDraw 4.5 chemical structure of ΔFd. (C) CD spectra of ΔFd, $(\Delta Fm)_2$, and D-Lys-ΔFd (6 μM each) in 20 mM SDS/10 mM sodium phosphate buffer (pH 7.5). (D) Chemical structures of ΔPhe, Phe, and α-Aib.

bacterial strains (*9*) have revealed that a rather simple amphipathic cationic character confers antimicrobial specificity to Nature's antibiotic peptides. Although some investigators have proposed destruction of the cytoplasmic membrane permeability barrier as the main mode of action, others have shown that AMPs have intracellular cytoplasmic targets (*10*). However, in spite of several investigations, the bacteriostatic and bactericidal actions of most AMPs have eluded comprehensive understanding. In this study, we have used protein and nonprotein amino acid-based de novo peptide design on a constant template of cationic amphipathicity to delineate the factors that influence AMP action. The nonprotein conformationally constrained amino acids used here include α-aminoisobutyric acid (α-methylalanine) and didehydrophenylalanine (Figure 1D). A double bond between α- and β-carbon atoms characterizes the didehydro amino acids. This simple modification imparts dramatic changes in the conformational and biochemical properties of the peptides harboring them. Didehydro and dialkyl amino acid residues are frequently found in naturally occurring peptides of fungal and microbial origin. Didehydro amino acids are also constituents of the lantibiotic class of polycyclic peptide antibiotics such as nisin, epidermin, subtilin, etc. (*11*). A major thrust of our studies is reporting the significant impact of dimerization on the advent or augmentation of antimicrobial potency in a wide spectrum of de novo designed peptides. Dendrimerization as a means of designing potent antimicrobials has engaged the attention of only a few laboratories in the past. In the earliest studies by Tam *et al.* (*12*), showing the enhancement of the activity of antimicrobial peptides by dendrimerization, an asymmetric lysine branch formed the dendrimeric core tethered with two to eight copies of a tetra- or octapeptide. The activity of these dendrimeric peptides was shown to be higher under both low- and high-salt conditions than the activity of the corresponding linear peptides with units of the peptide linked in a linear mode. Further, compared to their linear counterparts, the branched peptides were found to be more water-soluble, more stable to proteolysis, less toxic to human cells, and more easily synthesized (an advantage of dendrimeric over linear peptides of comparable size is that they require far fewer steps in their chemical synthesis). It was suggested that the augmentation of activity due to dendrimerization was a consequence of the increase in the effective molarity of the monomeric units and a decrease in the entropy of self-assembly. More recently, Liu *et al.* (*13*) used the reactive polymaleic anhydride chain for linking antimicrobial tetrapeptides to obtain multivalent variants containing approximately 40 monomer units. Relative to the free peptides, these dendrimers exhibited 10-fold improvement in antimicrobial potency. Likewise, Arnusch *et al.* (*14*) reported large increases in the pore forming abilities of tetra- and octavalent forms of magainin. Here, we report that branched dimeric peptides acting as scaffolds reveal the latent potential of their monomeric counterparts. We have used four different branched dimeric peptides to show that both the dimeric motif and the characteristics of the monomer sequence used for dimerization influence the potency and the spectrum of antibiotic action. In comparing the antimicrobial properties of linear dimer $(\Delta Fm)_2$ versus lysine-branched dimer ΔFd, we have observed that both dimers are nearly equipotent against *Escherichia coli*. However, against *Staphylococcus aureus*, the branched dimer is 4-fold more potent than the linear dimer. We present a detailed analysis of the antimicrobial action of the lysine-branched dimeric didehydrophenylalanine-containing amphipathic, helical AMP in the creation of a novel potent broad-spectrum antimicrobial peptide pharmacophore. Our study has revealed that antibiotics designed

for potent targeting of both the membrane and the cell interior simultaneously rather than sequentially are likely to show strong and broad-spectrum antimicrobial effects across Gram-negative and Gram-positive bacteria.

EXPERIMENTAL PROCEDURES

Materials. Amino acid derivatives and resin for peptide synthesis were from Nova Biochem. *N*,*N*′-Diisopropylcarbodiimide (DIPCDI), piperidine, dimethylformamide (DMF), dichloromethane (DCM), *N*-hydroxybenzotriazole (HOBT), isobutylchloroformate (IBCF), trifluoroacetic acid (TFA), triisopropylsilane (TIS), DL-*threo*-*β*-phenylserine, sodium hydroxide, citric acid, fluorescein 5-isothiocyanate (FITC), 3-(4,5-dimethylthiazol-2-yl)-2,5-diphenyltetrazolium bromide (MTT), dimethyl sulfoxide (DMSO), polymyxin B sulfate (PXB), LPS (*E. coli* serotype 055:B5), glucose, and HEPES were from Sigma Chemical Co. *N*-Methylmorpholine (NMM) and 1-*N*-phenylnaphthylamine (NPN) were from Aldrich. Sodium chloride, acetic anhydride, and tetrahydrofuran (THF) were from Qualigens. Ethyl acetate, sodium acetate, and sodium sulfate were from Merck. Silica gel TLC plates (60F-254) were from Merck. Mueller Hinton (MH) broth and Bacto agar were from Difco. Dulbecco's modified Eagle's medium (DMEM) and fetal bovine serum (FBS) were from Gibco. Dansyl chloride was from Calbiochem (San Diego, CA). Propidium iodide (PI) and Syto 9 were from Molecular Probes (Eugene, OR).

Preparation of Fmoc-X-ΔPhe Azalactones. These were synthesized from their respective Fmoc-X-DL-*threo*-*β*-phenylserine [X = Gly, Lys (Boc), Ala] derivatives as described previously (*15*). TLC, mass spectroscopy, and UV−visible spectroscopy were used to confirm the authenticity and purity of the azalactones.

Peptide Synthesis. Peptides were synthesized as C-terminal amides using standard Fmoc chemistry on Rink amide MBHA resin in the manual mode using DIPCDI and HOBT as coupling agents. In the case of branched dimers, Fmoc-Lys(Fmoc)-OH was first coupled to the resin to make a branching core. The removal of both Fmoc protecting groups with 20% piperidine and DMF from Fmoc-Lys(Fmoc)-resin gave rise to two (α and ε) amino groups for simultaneous synthesis of two identical chains of the same peptide (Figure 1B). Both coupling of amino acid and Fmoc deprotection were monitored by Kaiser test (*16*). Standard chemical methods described in the Supporting Information were used for side chain protections, acetylation or FITC labeling of the N-terminus, cleavage of peptides from resin, and postcleavage workup. The yields of solid phase synthesis-derived peptides used in this study were typically >90% (crude) and 50−60% (purified). The identity of peptides was confirmed by mass spectrometry. All peptides used in this study had a RPHPLC [column, Novapak C18, 4 μm, 4.6 mm × 250 mm, flow rate of 1 mL/min, solvent system of water/acetonitrile with 0.1% TFA, gradient from 5 to 75% acetonitrile over 70 min (1% acetonitrile/min)] purity of >95%. The mass spectroscopy data for peptides are shown in Figures 8 (Fm, ΔFm, and Um), 9 (ΔFd, Ud, D-Lys-ΔFd, and Fd), 10 [$(\Delta Fm)_2$], 11 (FITC-ΔFm, FITC-Um, and FITC-ΔFd), and 12 (FITC-Ud and FITC-D-Lys-ΔFd) of the Supporting Information. For structures and abbreviations of each parent peptide used in the study, please refer to Table 1.

Antibiotic Susceptibility Testing. (i) Minimum Inhibitory Concentrations (MICs). The MICs were determined against *E. coli* ML35p and vancomycin/methicillin resistant *S. aureus* ATCC 700699 according to the Modified MIC Method for Cationic Antimicrobial Peptides (*17*). Bacteria grown overnight were diluted in MH broth to a cell density of 10^5 CFU/mL; 100 μL of this culture was aliquoted into the wells of a 96-well microtiter plate (Costar, Corning Inc., Corning, NY), and 11 μL of 10× stocks of different peptides (in 0.2% BSA and 0.01% acetic acid) was added. This mixture was incubated (37 °C and 200 rpm) in a rotary shaker incubator (Kuhner, Basel, Switzerland). After incubation for 18 h, A_{600} was measured in a microtiter plate reader (VERSA max tunable, Molecular Devices, Sunnyvale, CA). The MIC is defined as the lowest concentration of a drug that inhibits measurable growth of an organism after overnight incubation. Peptide concentrations were determined spectrophotometrically at 280 nm (ε_{280} = 5050 and 19000 M^{-1} cm^{-1} for tryptophan and ΔF, respectively). The concentration of FITC-labeled peptides was determined using FITC absorbance at 495 nm ($\varepsilon_{495} = 7.7 \times 10^4$ M^{-1} cm^{-1}). Each experiment was conducted in triplicate and was repeated at least twice.

(ii) Minimum bactericidal concentrations (MBCs) were determined by plating 100 μL from each clear well of the MIC experiment on MH agar plates in triplicate. After incubation (37 °C for 18 h), the MBC was identified as the lowest concentration that did not permit growth of 99.9% bacteria on the agar surface.

Kinetics of Inhibition of Growth of E. coli by Various Peptides. *E. coli* ML35p cells were incubated with peptides, and the antibiotic susceptibility procedure described above in Antibiotic Susceptibility Testing (i) Minimum Inhibitory Concentrations (MICs) was followed. At different time intervals, the microtiter plate was taken out of the rotary shaker incubator and readings were taken in the microtiter plate reader at 600 nm. Data shown are the average from triplicate wells.

Killing Kinetics at 4 × MIC. *E. coli* ML35p cells grown overnight were diluted in MH broth to a cell density of 10^5 CFU/mL. One milliliter of this cell suspension was incubated with 4 × MIC of the respective peptide [ΔFm (440 μM), ΔFd (10 μM), Fd (12 μM), Ud (120 μM), and D-Lys-ΔFd (20 μM)] or water (in the case of control) and incubated in Eppendorf microfuge tubes (37 °C and 200 rpm) in a rotary shaker. At different time points (0, 5, 20, and 60 min), a 100 μL aliquot was withdrawn, diluted in 10-fold dilutions using MH broth, and plated on MH agar plates. The plates were incubated (37 °C for 20 h) and colonies counted.

Table 1: Primary Structures of Monomeric and Dimeric Peptides Studied for Antimicrobial Action

	abbreviation	structure
1	*Um*	Ac-G-*U*-R-K-*U*-H-K-*U*-W-A-NH_2
2	*Fm*	Ac-G-*F*-R-K-*F*-H-K-*F*-W-A-NH_2
3	*ΔFm*	Ac-G-*ΔF*-R-K-*ΔF*-H-K-*ΔF*-W-A-NH_2
4	$(\Delta Fm)_2$	Ac-G-*ΔF*-R-K-*ΔF*-H-K-*ΔF*-W-A-A-G-*ΔF*-R-K-*ΔF*-H-K-*ΔF*-W-A-NH_2
5	*ΔFd*	Ac-G-*ΔF*-R-K-*ΔF*-H-K-*ΔF*-W-A-K NH_2 Ac-G-*ΔF*-R-K-*ΔF*-H-K-*ΔF*-W-A⁄
6	*D-Lys-ΔFd*	Ac-G-*ΔF*-R-K^D-*ΔF*-H-K^D-*ΔF*-W-A-K-NH_2 Ac-G-*ΔF*-R-K^D-*ΔF*-H-K^D-*ΔF*-W-A⁄
7	*Fd*	Ac-G-*F*-R-K-*F*-H-K-*F*-W-A K-NH_2 Ac-G-*F*-R-K-*F*-H-K-*F*-W-A⁄
8	*Ud*	Ac-G-*U*-R-K-*U*-H-K-*U*-W-A-K-NH_2 Ac-G-*U*-R-K-*U*-H-K-*U*-W-A⁄

Dansyl Polymyxin B Displacement Assay. The relative binding affinity of each peptide for LPS was determined by the dansyl polymyxin B displacement assay (*18*). Peptides at different concentrations were individually titrated into a cuvette containing 3 μg of LPS/mL and dansyl PXB (an amount that resulted in 85−90% saturation of LPS binding sites) in 10 mM sodium phosphate buffer (pH 7.5). The decrease in fluorescence was used to calculate the percent displacement of dansyl PXB. Buffer blank was subtracted from peptide spectra. Spectra were recorded on a Perkin-Elmer LS-50B spectrofluorimeter using a cuvette with a path length of 1 cm. The excitation and emission wavelengths were 340 and 350−600 nm, respectively, and the corresponding slit widths were 5 and 10 nm, respectively. Each data point represents the mean and standard deviation of three independent observations.

Hemolytic Activity Testing. Hemolytic activity was tested as described previously (*19*). Human blood with 10% citrate phosphate dextrose was obtained from the Rotary Blood Bank (New Delhi, India). Red blood cells (RBCs) harvested by spinning (1000*g* for 5 min at 25 °C) were washed three to five times with phosphate-buffered saline (PBS). The packed cell volume obtained was used to make a 2% (v/v) suspension in PBS. This RBC suspension (96 μL) was transferred to each well of a microtiter plate and mixed with 4 μL of peptide solutions at the desired concentration. The plate was incubated (37 °C for 60 min) in an incubator with no shaking and centrifuged (1000*g* for 5 min at 25 °C). Supernatant (50 μL) was transferred to new wells, and OD_{414} was measured on a microtiter plate reader to monitor RBC lyses. RBCs suspended in PBS and RBCs lysed using 0.1% Triton X-100 acted as negative and positive controls, respectively. Each data point represents the mean and standard deviation of three independent observations.

Outer Membrane Permeabilization Assay. The outer membrane permeabilization activity of the peptides was determined by the NPN assay (*20*). Midlog phase (OD_{600} = 0.5, 2×10^8 CFU/mL) *E. coli* ML35p cells, harvested by centrifugation (4000 rpm and 4 °C for 10 min) were washed and resuspended at the same cell density in 5 mM glucose/5 mM HEPES buffer (pH 7.2). Ten microliters of a 250× concentration of peptides in water was added to a cuvette containing 2.5 mL of cell suspension and 10 μM NPN (50 μL from a 500 μM stock in acetone). Excitation and emission were at 350 nm (slit width of 5 nm) and 420 nm (slit width of 10 nm), respectively. The uptake of NPN as a measure of outer membrane permeabilization was monitored by the increase in the fluorescence of NPN. Each data point represents the mean and standard deviation of three independent observations.

PI Uptake-Based Assay and FACS Analysis. *E. coli* ML35p cells grown overnight were subcultured (OD_{600} = 0.35, 1×10^8 CFU/mL), harvested by centrifugation (4000 rpm for 10 min at 4 °C), washed, and resuspended in 5 mM HEPES buffer (pH 7.2) to yield 10^8 CFU/mL. Fifteen microliters of cell suspension was added to 135 μL of 5 mM HEPES buffer (pH 7.2) containing PI (3 μL, 1 mg/mL) and peptide at different concentrations. The mixture was incubated (15 min at room temperature) and then subjected to FACS (FACSCalibur, Becton Dickinson). FACS data were analyzed using FlowJo version 8.5.2 (Tree Star Inc., San Carlos, CA). Untreated cells with or without PI served as a control.

PI and Syto 9 Uptake-Based Fluorescence Microscopic Analysis of Cell Permeabilization by Peptides. *E. coli* ML35p cells grown were overnight subcultured to an OD_{600} of 0.35 (1×10^8 CFU/mL). Cells were harvested by centrifugation (4000 rpm for 10 min), washed, and resuspended in 5 mM glucose/10 mM sodium phosphate buffer (pH 7.5) to yield 10^8 CFU/mL; 100 μL of *E. coli* suspensions (10^8 CFU/mL) were incubated with 2 μL from respective peptide aqueous stock solutions to yield a final peptide concentration of 100 μM (Um, Fm, and ΔFm), 30 μM (Ud), 2.5 μM (ΔFd), 5 μM (D-Lys-ΔFd), and 3 μM (Fd) for 150 min and 18 h at 37 °C and 200 rpm in Kuhner rotary shaker incubator. Ten microliters of each sample was incubated with PI (2.7 μM) and Syto 9 (6 μM) for 15 min. A smear was made, heat-fixed, and visualized under a Nikon fluorescence microscope under PI and Syto 9 filters. Cells without peptide served as a control.

Scanning Electron Microscopy. *E. coli* ML35p cells grown overnight were subcultured, harvested by centrifugation (4000 rpm for 10 min at 4 °C), and resuspended in 5 mM HEPES buffer (pH 7.2) to yield 10^8 CFU/mL. Fifteen microliters of this cell suspension was mixed with peptides (ΔFm and ΔFd at their respective MICs and Um and Fm at 110 μM) in 135 μL of 5 mM HEPES buffer (pH 7.2). The mixture was incubated with shaking (200 rpm and 37 °C) for 15 min. Cells were spun down (4000 rpm and 4 °C for 10 min), washed thrice in 0.1 M phosphate buffer (pH 7.4), and fixed in modified Karnovsky's fluid (*21*) [buffered with 0.1 M phosphate buffer (pH 7.4)] at 4 °C for 2 h. They were next washed in fresh buffer and dehydrated with graded ethanol (30, 50, 70, 90, and 100%). The samples were treated (2 × 5 min) with hexamethyldisilizane (SRL, Mumbai, India) and air-dried in a desiccator. An Automatic Sputter coater (Agar Scientific, Essex, England) was used for coating the specimens with 15 nm gold particles. After being processed, the samples were observed via SEM on a LEO 435 VP. The images were processed using Photoshop 6.0 (Adobe Systems, San Jose, CA).

Transmission Electron Microscopy. *E. coli* ML35p cells grown overnight were subcultured (OD_{600} = 0.35, 1×10^8 CFU/mL), and 2 mL of cells was suspended in 20 mL of fresh medium to which 200 μL of 250 μM ΔFd had been added. Cells were incubated on a shaker (37 °C and 200 rpm) with ΔFd (75 min). Cells in medium without peptide were used as a control. After the desired incubation time, cells were harvested by centrifugation (4000 rpm for 10 min at 4 °C), washed thrice with 0.1 M phosphate buffer (pH 7.4), and fixed in modified Karnovsky's fluid (*21*) buffered with 0.1 M phosphate buffer (pH 7.4) at 4 °C for 2 h. Following the wash in fresh buffer, they were postfixed (glutaraldehyde fixes only proteins, and unsaturated lipids may be fixed using osmium tetroxide following glutaraldehyde fixation; this procedure is called postfixation) for 2 h at 4 °C. After several washes in 0.1 M phosphate buffer, the sample was dehydrated in graded acetone solutions and embedded in CY212 Araldite. Ultrathin sections were cut using an ultra cut E (Reichert Jung, Depew, NY) ultra microtome, and the sections were stained in alcoholic uranyl acetate and lead citrate before being examined on the grids in a transmission electron microscope (Fel; Morgagni 268 D TEM) operated at 80 kV.

Cellular Uptake of Peptides Studied by Fluorescence Microscopy. *E. coli* ML35p cells grown overnight were subcultured to an OD_{600} of 0.35 (1×10^8 CFU/mL). Cells were harvested by centrifugation (4000 rpm for 10 min), washed, and resuspended in 5 mM glucose/10 mM sodium phosphate buffer (pH 7.5) to yield 10^8 CFU/mL; 100 μL of *E. coli* suspensions (10^8 CFU/mL) was mixed with 5 μL of the respective FITC-labeled peptide aqueous stock solutions to yield a final peptide concentration of 100 μM (ΔFm), 30 μM (Ud), or 5 μM (ΔFd, D-Lys-ΔFd, and Fd) and incubated (37 °C and 200 rpm) for

different periods of time (5, 15, 30, and 150 min and 18 h) in Kuhner rotary shaker incubator. Cells were harvested by centrifugation (4000 rpm for 10 min) and washed twice with 5 mM glucose in 10 mM sodium phosphate buffer (pH 7.5). A smear was made, heat-fixed, and visualized under a Nikon fluorescence microscope. For confocal microscopy, confocal laser scanning (Radiance 2100, Bio-Rad) under a Nikon microscope (objective plane Apo 60×/1.4 oil) was used to observe the slide. The excitation wavelength for FITC was 494 nm (argon laser), and fluorescence was detected through an HQ 515/30 emission filter (high-quality band-pass). Image processing was conducted with Lazer Sharp (Bio-Rad), and Photoshop 6.0 (Adobe Systems, San Jose, CA) was used for the final image assembly.

CD Spectroscopy. CD experiments were performed on a Jasco J-810 spectropolarimeter with a 1 mm path length cuvette. Spectra were acquired between 190 and 340 nm at 25 °C (scan speed of 200 nm/min, response time of 4 s, bandwidth of 1 nm). Five spectra were collected and averaged.

Salt Tolerance. The method described for MIC determination was used except that salt from a concentrated NaCl stock solution in water was added to 100 μL cultures in MH broth to yield the desired salt concentration.

Proteolytic Stability of Peptides to Trypsin and Chymotrypsin. Peptides and trypsin/chymotrypsin (Figure 4 of the Supporting Information), taken at a ratio of 100:0.5 (molar ratio) in 0.1 M ammonium bicarbonate and 0.1 mM $CaCl_2$ (pH 8.3), were incubated in a rotary shaker incubator (37 °C and 200 rpm for 30 min). An aliquot was injected into the RPHPLC system [C18 column, particle size of 4 μm, gradient of 5 to 75% acetonitrile with 0.1% trifluoroacetic acid over 70 min (1% acetonitrile/min), flow rate of 1 mL/min, detector at 214 nm]. Untreated peptides processed in the same manner as enzyme-treated samples served as controls. Identical amounts of control and protease-treated samples were injected into the RPHPLC system. For the variable time-dependent assay (Figure 5 of the Supporting Information), peptides were incubated with enzyme for 0, 1, and 2 h.

RPHPLC Study of Uptake of Peptides by Bacteria. *E. coli* ML35p cells grown overnight were subcultured to an OD_{600} of ~0.4 (10^8 CFU/mL). Cells were harvested by centrifugation (4000 rpm for 10 min at 4 °C) and resuspended in 250 μL of 10 mM sodium phosphate buffer (pH 7.5). They were incubated with the respective peptides (625 μM) in a total volume of 300 μL on a rotary shaker incubator (200 rpm and 37 °C for 30 min) and spun (4000 rpm for 10 min), and the supernatant (270 μL) was mixed with equal volume of 10% acetonitrile and 0.2% TFA. The mixture was spun (13000 rpm for 10 min), and 520 μL of supernatant was taken for RPHPLC analysis. The cell pellet was washed and centrifuged and the supernatant processed and analyzed as described above. Cells were sonicated [Sonics Vibra Cell, Sonics & Materials Inc., Newtown, CT (setting at 25% amplitude, pulse on and off for 9.0 s each for 2 min)] on ice in 10 mM sodium phosphate buffer (pH 7.5) using a microprobe. This sonicate was centrifuged (12000 rpm and 4 °C for 1 h) and the supernatant processed and analyzed as described above. Loading 520 μL into a 500 μL loop ensured precise 500 μL injections.

RPHPLC Study of the Interaction of Peptides with Bacterial Cytosol. Midlog phase *E. coli* ML35p cells (2×10^8) were sonicated in 300 μL of 10 mM sodium phosphate buffer (pH 7.5) exactly as described above. The spun supernatant (12000 rpm for 1 h at 4 °C) was mixed with individual peptides added to a final concentration of 625 μM. The observed precipitate was spun to obtain supernatant A (270 μL). The pellets were washed with 300 μL of 10 mM sodium phosphate buffer (pH 7.5) and spun (10000 rpm for 15 min at 4 °C) to yield supernatant B. The washed pellets were dissolved in 0.1% TFA (300 μL) and spun to yield supernatant C. All supernatants (A−C) were analyzed by RPHPLC as described above.

HeLa Cell Cytotoxicity. HeLa cell cytotoxicity was tested as described previously (*22*). HeLa cells in 96-well microplates (5×10^5 cells/well) were cultured overnight in Dulbecco's modified Eagle's medium containing 10% fetal bovine serum. After removal of the medium, cells were mixed with 0.1 mL of peptides (ΔFm and ΔFd at their respective *E. coli* MICs, while Um and Fm were tested at the MIC of ΔFm) and incubated (37 °C for 24 h). Ten microliters of a 5 mg/mL MTT solution in PBS was added, and the cells were incubated for 2 h at 37 °C. Thereafter, dimethyl sulfoxide (DMSO) (0.1 mL) was added to dissolve the formazan crystals formed by MTT reduction. Cells without peptide treatment served as a control. The ratio of OD_{590} for peptide-treated cells to OD_{590} for untreated cells was used to calculate the percent viability of cells.

Gel Retardation Assay. ΔFm and ΔFd (1 μL) from the respective stock solutions [20 and 50 ng/μL (for ΔFm) and 8, 2, and 1 ng/μL (for ΔFd)] made to provide the indicated amounts of each peptide were mixed with 1 μL of ^{32}P-end-labeled DNA (16 bp probe, 1 ng/μL) and incubated for 5 min at room temperature on Parafilm. The 6× loading dye (xylene cyanol and bromophenol blue, 2.5 mg each in 1 mL of 25% glycerol) (10 μL) was added to the samples which were then loaded on a 15% nondenaturing PAGE gel. After electrophoresis (15 mA for 120 min), the gel was dried in a Bio-Rad model 583 gel dryer, exposed overnight in a Phosphoimager cassette (Amersham Biosciences), and scanned in Typhoon 9210 Variable Mode Imager. The DNA probe used was 5′-CCUCUCTG-GACCTTCC-3′·3′-GGAGAGACCTGGAAGG-5′.

SDS−PAGE Study of the Precipitation of Cellular Proteins by Peptides. *E. coli* ML35p cells grown overnight were subcultured (OD_{600} = 0.32, 1×10^8 CFU/mL) and cells harvested from a 10 mL culture by centrifugation (4000 rpm for 10 min at 4 °C). The cell pellet was washed with 10 mL of HEPES buffer (5 mM, pH 7.2), resuspended in 300 μL of the same buffer, and sonicated as described previously. The sonicate was spun (12000 rpm and 4 °C for 1 h). To 200 μL of sonicate supernatant was added 100 μL of desired peptide solutions in water to give the final peptide concentrations (5−200 μM) indicated in Figure 7B. A visible precipitate was spun down (12000 rpm for 10 min at 4 °C) and washed with 5 mM HEPES buffer (pH 7.2, 300 μL). Pellets were boiled (5 min) in SDS- and β-mercaptoethanol-containing sample buffer and loaded on a 12% SDS−PAGE gel. Following electrophoresis, the gel was stained with silver. As controls, the same protocol was followed with Src peptide (HRLIEDAHYAARG), NS4 (AIFASRGNHVSPTHYV), and Oxytocin (H-CYIQNCPLG-NH_2) (1−6 S−S). These peptides had expected and (observed) molecular weights of 1371.5 (1371.9), 1755.9 (1756.4), and 1007.19 (1007.8), respectively.

RESULTS

De Novo Design of Antimicrobial Peptides. The prototypic decapeptide Ac-GXRKXHKXWA-NH_2 was designed to provide cationic amphipathic peptides. The segregation of positively charged lysines and arginine from the apolar X residues

[α-aminoisobutyric acid (U)/phenylalanine (F)/α,β-didehydrophenylalanine (ΔF)] in the 3_{10}-helical wheel diagram (Figure 1A) illustrates the two faces of such an amphipathic helix. U (aliphatic) and ΔF (aromatic) have been incorporated since these nonprotein amino acids have proven ability to induce 3_{10}-helical folds in peptides (*23*, *24*). Circular dichroism analysis of Um and ΔFm indeed showed these peptides to have ordered structures in SDS (Figure 1 of the Supporting Information). The 3_{10}-helix conformation for ΔFm is evident from the strong excitonic couplet at 267 and 298 nm with a crossover at 280 nm (*25*). A 3_{10}-helix conformation for Um is evident from the stronger minimum at 206 nm than the one at 226 nm (*26*, *27*). The Fm peptide, which exhibited a positive peak at 196 nm and a negative peak at 226 nm in water, also seems to acquire a more rigid although undefined structure in SDS. Branched dimers ΔFd, Ud, and Fd of Ac-GXRKXHKXWA-NH_2 (X is ΔF, U, or F) were assembled using the α- and ε-amino groups of lysine as described in Experimental Procedures. Figure 1B shows the chemical structure of ΔFd. A diastereoisomeric analogue of ΔFd having four of its lysine residues in the D-configuration was also synthesized (see Table 1). Since the D-lysines were introduced to act as helix terminators, this peptide designated as D-Lys-ΔFd was expected to be nonhelical. As is characteristic of ΔF-containing peptide helices, ΔFd exhibited a strong excitonic couplet via circular dichroism (Figure 1C). In contrast, the nonhelical isomeric peptide D-Lys-ΔFd lacked such a couplet. Therefore, D-Lys-ΔFd is a close molecular mimic of ΔFd without its helicity. To determine if the antibiotic action of the dimer may depend on the mode of dimerization, we also synthesized a linear dimer of ΔFm, viz. $(\Delta Fm)_2$. This 21-residue linear dimer with six ΔF residues (Table 1) was expected to be helical. Indeed, the CD spectrum of $(\Delta Fm)_2$ (Figure 1B) exhibits a 3_{10}-helix-associated excitonic couplet with characteristics similar to those of the excitonic couplet shown by ΔFd. However, the 2- and 4-fold lower molar ellipticities of the 267 and 298 nm bands, respectively, in $(\Delta Fm)_2$ vis-à-vis ΔFd suggest that the branched dimer makes a stronger helix than the linear dimer.

Selectivity in Action of Antimicrobial Peptides. Inherent in the design of antimicrobial peptides is the notion that the prokaryotic microbes are significantly different from the eukaryotic mammalian cells. It is interesting that the highest degree of distinction between eukaryotes and prokaryotes is at the very surface of the respective cell types: while microbes present a largely anionic exterior, the surface of eukaryotic cells is essentially neutral (*28*). To examine how the prokaryote−eukaryote selectivity parameters change in structurally altered peptides, we determined their antimicrobial potency against Gram-positive and Gram-negative bacteria, hemolytic activity against human red blood cells, and cytotoxic activity against HeLa cells. As shown (Table 2), of the three monomeric peptides (ΔFm, Fm, and Um), only ΔFm was modestly antibiotic against the Gram-negative *E. coli* (MIC of 110 μM, MBC of 500 μM) and quite inactive against the Gram-positive *S. aureus* (MIC of 450 μM, MBC of > 500 μM). None of these peptides showed any significant hemolytic or cytotoxic activity.

Dimerization of ΔFm Potentiates Antimicrobial Action. Interestingly, the lysine-branched dimerization of ΔFm to ΔFd led to an ~100-fold increase in antibiotic potency against *E. coli* (MBC of 5 μM) and the advent of a nearly equipotent antibiotic action against vancomycin/methicillin resistant *S. aureus* [MBC of 7.5 μM (Table 2)]. Furthermore, these desired effects occurred with retention of selectivity against bacteria since at its MIC, ΔFd

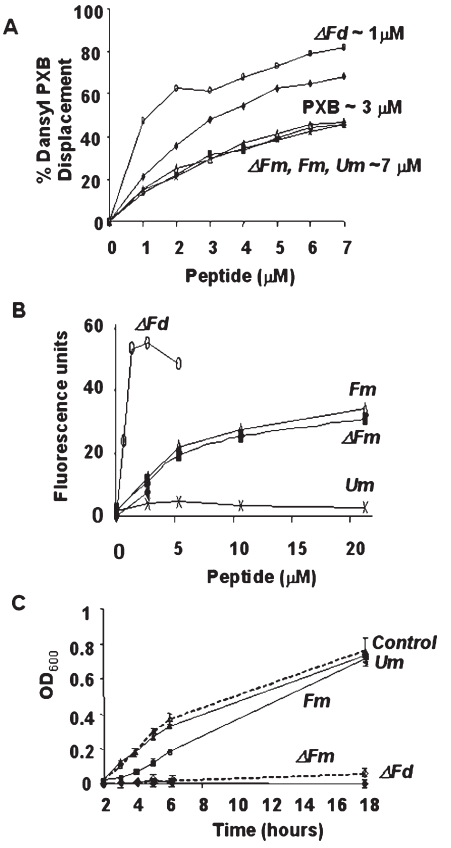

FIGURE 2: (A) Dansyl polymyxin B assay of peptide−LPS binding. Numbers against each peptide indicate I_{50} values. (B) Peptide-induced *E. coli* ML35p outer membrane permeabilization NPN assay. (C) Growth kinetics of *E. coli* ML35p in the absence (control) and presence of Fm, ΔFm, and Um (110 μM each) and ΔFd (2.5 μM). Each data point in panels A−C represents the mean and standard deviation of three independent observations.

was neither significantly hemolytic nor cytotoxic. ΔFd exhibited only marginal (~ 2%) hemolytic activity even at 10 times its MBC (Figure 2 of the Supporting Information). To determine if the antimicrobial potencies of the dimeric molecule may be influenced by the mode of dimerization, we examined the antimicrobial properties of the linear dimer $(\Delta Fm)_2$. As shown (Table 2), while both the linear and branched dimers were nearly equipotent against *E. coli*, the branched dimer was significantly more potent than the linear dimer against *S. aureus*.

Dimerization of Fm and Um Also Potentiates Antimicrobial Action. To determine if lysine-branched dimerization per se could be a motif that potentiates antimicrobial action, we examined the comparative potency and ambit of action profiles of all four dimers, viz. Ud, ΔFd, Fd, and D-Lys-ΔFd. As shown (Table 3), dimerization increased the antimicrobial potencies of Um and Fm as well. However, each dimer exhibited unique features of potency and targeting. Thus, Ud (*E. coli* MIC of 30 μM, MBC of 150 μM) was mildly active against *E. coli* but quite inactive against *S. aureus*, and Fd, although quite potent against *E. coli* (*E. coli* MIC of 3 μM, MBC of 6 μM), was rather weak against *S. aureus* (MIC and MBC of 45 μM each). The nonhelical dimer D-Lys-ΔFd exhibited a combination of low MIC (5 μM) and high MBC (25 μM) against *E. coli* and was quite inactive against *S. aureus* (MIC of 55 μM, MBC of 150 μM). In light of the realization that dimerization unravels the latent potential of monomeric peptides (Um, Fm, and ΔFm), and that ΔFd has the most promising antibiotic profile, we set out to find

Table 2: Amphipathic, Aromatic, Helical Branched Dimer as a Motif for Specific and Broad-Spectrum Antibacterial Action[a]

Peptide		*E.coli* ML35p			*S.aureus* ATCC 700699			Hemolysis (%)	HeLa cell toxicity (%) MTT assay
		MIC (μM)	MBC (μM)	MBC/MIC	MIC (μM)	MBC (μM)	MBC/MIC		
Helical aliphatic monomer Ac-G*U*RK*U*HK*U*WA-NH_2	*1178 *Um*	>500	>500	-	>500	>500	-	0	0
Random aromatic monomer Ac-G*F*RK*F*HK*F*WA-NH_2	*1364 *Fm*	>500	>500	-	>500	>500	-	0	0
Helical aromatic monomer Ac-G*Δ F*RK*Δ F*HK*Δ F*WA-NH_2	*1358 *ΔFm*	110	500	4.5	450	>500	-	0	7
Linear aromatic dimer Ac-X-A-X-NH_2 X= G*Δ F*RK*Δ F*HK*Δ F*WA	*2729 *(ΔFm)₂*	2	2	1	20	20	1	ND	ND
Helical aromatic dimer Ac-G*Δ F*RK*Δ F*HK*Δ F*WAK-NH_2 Ac-G*Δ F*RK*Δ F*HK*Δ F*WA	*2828 *ΔFd*	2.5	5	2	5	7.5	1.5	0	4

[a] The % hemolysis and % HeLa cell toxicity have been studied at the *E. coli* MICs of the respective peptides. Peptides with a MIC of > 110 μM have been studied at 110 μM. ND means not done. * Numbers represent molecular weights in Daltons. The residues characteristic to each peptide have been italicized.

Table 3: Comparative Antimicrobial Profiles of Dimeric Peptides[a]

Peptide dimer		*E.coli* ML35p			*S.aureus* ATCC 700699			MIC *S.aureus* / MIC *E.coli*	MBC *S.aureus* / MBC *E.coli*
		MIC (μM)	MBC (μM)	MBC/MIC	MIC (μM)	MBC (μM)	MBC/MIC		
Helical aliphatic dimer Ac-G*U*RK*U*HK*U*WA-K-NH_2 Ac-GURKUHKUWA	2467 *Ud*	30	150	5	>100	-	-	-	-
Non-Helical aromatic dimer Ac-G*Δ F*RK^D*Δ F*HK^D*Δ F*WAK-NH_2 Ac-G*Δ F*RK^D*Δ F*HK^D*Δ F*WA *D-Lys-ΔFd*	2828	5	25	5	55	150	2.7	11	6.0
Barely Helical aromatic dimer Ac-G*F*RK*F*HK*F*WA-K-NH_2 Ac-G*F*RK*F*HK*F*WA *Fd*	2840	3	6	2	45	45	1	15	7.5
Linear Helical aromatic dimer Ac-X-A-X-NH_2 X= G*Δ F* RK*Δ F*HK*Δ F*WA *(ΔFm)₂*	2729	2	2	1	20	20	1	10	10
Branched Helical aromatic dimer Ac-G*Δ F*RK*Δ F*HK*Δ F*WAK-NH_2 Ac-G*Δ F*RK*Δ F*HK*Δ F*WA *ΔFd*	2828	2.5	5	2	5	7.5	1.5	2	1.5

[a] Underlined numbers in the first column represent molecular weights in Daltons.

the distinctive features of the action of monomers and their corresponding dimers.

Binding of Cationic Monomeric Peptides versus Dimeric ΔFd to LPS. The polyanionic LPS is known to form an effective permeability barrier (*29*) and play a major role in the resistance of Gram-negative bacteria to toxic agents (*30*). As a signature of the outer surface of Gram-negative bacteria, it also provides a high-avidity, high-affinity launching pad for amphipathic cationic AMPs. The characteristics of binding of ΔFm, Um, Fm, and ΔFd to LPS in a dansyl polymyxin B (PXB) assay (*31*) are shown in Figure 2A. The three monomeric peptides which possess three sequentially equivalent positive charges appeared to have identical affinities ($I_{50} \sim 7$ μM) for LPS. In contrast, ΔFd with six positive charges and an I_{50} of ~1 μM turned out to have a far stronger affinity for LPS than its corresponding monomer. PXB (charge of +5) revealed an LPS binding affinity intermediate between those of the monomeric peptides (+3) and the dimer ΔFd (+6). It is apparent that ionic interactions play a dominant role in the binding of cationic AMPs to LPS. The cooperativity of ionic interactions between LPS and cationic peptides is expected to be much higher in ΔFd (charge of +6) as compared to ΔFm (charge of +3) and may explain the 7-fold higher affinity of ΔFd over ΔFm. The determinant role of cooperative ionic interactions was also seen in the differential salt tolerance of antibiotic actions of ΔFm versus ΔFd. Thus, at MIC, the I_{50} values of sodium chloride-mediated inhibition of antibiotic effects were found to be 25 and 75 mM for ΔFm and ΔFd, respectively (Figure 3 of the Supporting Information).

In the Absence of Aromaticity, Binding to LPS Is Not Sufficient To Cause Outer Membrane Permeabilization. As a result of the initial electrostatic attraction between cationic amphipathic AMPs and the negatively charged outer membrane of Gram-negative bacteria, these peptides are known to initiate not only the uptake of fluorescent dyes but also their own passage across the outer membrane through a "self-promoted uptake" mechanism (*31*). They facilitate their own uptake since, because of their stronger affinity for LPS, they displace the native divalent cations like Mg^{2+} and Ca^{2+} from LPS. However, substitution of the tiny inorganic ions by the much larger cationic peptides causes areas of instability in the outer membrane leading to

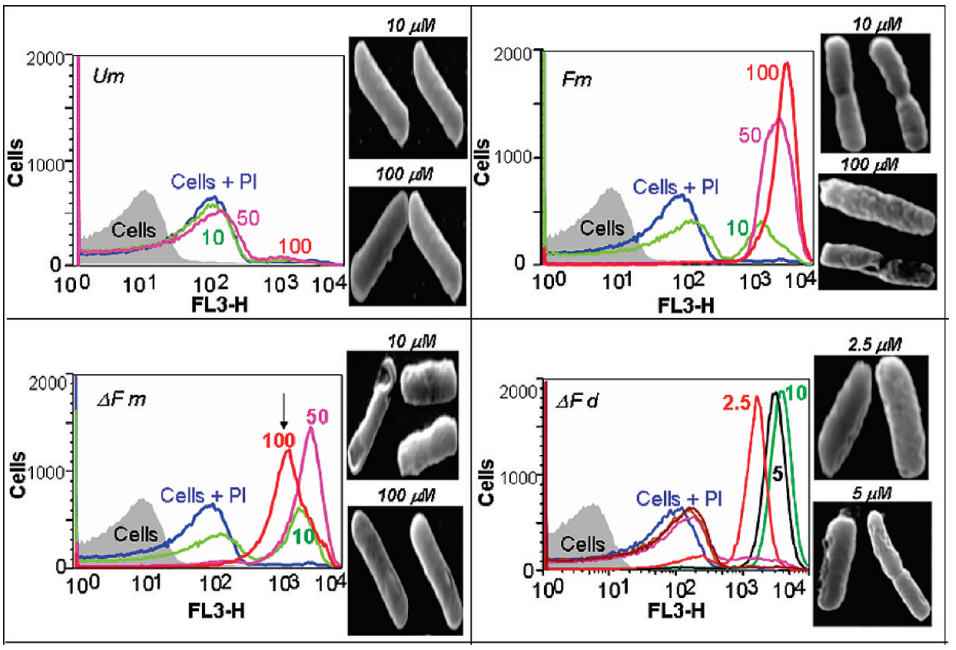

FIGURE 3: Differential effects of peptides on *E. coli* ML35p membrane architecture (as seen by SEM) and inner membrane permeabilization of PI (as examined by FACS analysis). Numbers represent micromolar peptide concentrations. The dimeric peptide ΔFd is 10-fold more membrane active than the monomeric peptides Fm and ΔFm. The arrow (panel ΔFm) indicates the concentration at which an inverse relation between ΔFm concentration and uptake of PI is seen. Note the correlation between microscopic surface changes and the extent of permeabilization.

subsequent translocation of the peptides toward the inner membrane. The membrane destabilizing function of peptides was judged by their ability to permeabilize the outer membrane to 1-phenylnaphthylamine (NPN), a hydrophobic fluorescent probe molecule, which fluoresces strongly only in a hydrophobic environment like the interior of a membrane. Figure 2B shows the tendencies of Fm, ΔFm, Um, and ΔFd to permeabilize the outer membrane as assessed by the NPN assay. While the two richly aromatic peptides, viz. ΔFm and Fm, exhibited distinct membrane permeabilizing ability, the largely aliphatic Um failed to cause permeabilization. It is also interesting to see that as a membrane permeabilizer, the dimer ΔFd is significantly more potent than the monomers ΔFm and Fm.

Effects of Antibiotic Peptides on the Kinetics of Bacterial Growth. Despite identical LPS binding affinities and outer membrane permeabilizing abilities, ΔFm was clearly more potent than Fm (Table 2). To gather clues about the observed difference in MICs, we set out to check the time kinetics of bacterial growth in presence of Um, Fm, and ΔFm (110 μM each) and ΔFd at its MIC (2.5 μM). As shown (Figure 2C), both ΔFm and ΔFd suppressed bacterial growth almost completely between 2 and 6 h and up to 18 h. On the other hand, no growth inhibitory effect was seen in cells treated with Um. Fm, which appeared to be ineffective as an antibiotic in the MIC experiment (Table 2), revealed its growth inhibitory effect in the first 3 h time window followed by resumption of growth between 3 and 18 h. As we shall see later, this dichotomy in the action of Fm may be related to its protease sensitivity.

Increasing Concentrations of Fm versus ΔFm Exhibit Differential Effects on Inner Membrane Permeabilization and Membrane Architecture. To measure the comparative efficacies of Um, Fm, ΔFm, and ΔFd to permeabilize the inner membrane, we measured the cellular uptake of propidium iodide (PI) using FACS. It may be noted that only those cells whose membranes have been destabilized exhibit PI-dependent red fluorescence (*32*). As shown (Figure 3), Um did not show even the slightest permeabilization to PI. Consistent with this lack of a functional attribute, the scanning electron micrograph (SEM) image of Um-treated cells (Figure 3) showed very little alteration of membrane architecture. In contrast, the FACS analysis with Fm showed a dose-dependent linear increase in the level of permeabilization as reflected in the progressive increase in the fluorescence intensity of PI. This linearity was mirrored also in the corresponding SEM, where the level of membrane perturbation significantly increased with an increase in the peptide concentration from 10 to 100 μM. However, in the case of ΔFm, the PI fluorescence increased progressively in going from 10 to 50 μM but declined at a peptide concentration of 100 μM. Consistent with this FACS analysis, the results of SEM corroborated the destabilization of membranes at 10 μM and their nearly perfect rehabilitation at 100 μM. In accordance with its high antimicrobial potency, ΔFd exhibited a high degree of permeabilization at its MIC (2.5 μM). With the increase in the ΔFd concentration to 2 and 4 times the MIC, the level of permeabilization showed a progressive increase with no reversal of the kind seen with ΔFm. The same was observed in SEM where sustained membrane damage is evident with an increase in the peptide concentration in the case of ΔFd-treated cells.

Fluorescence Microscopic Time Kinetics of Membrane Permeabilization by Monomers versus Dimers. Fluorescence microscopy of the uptake of Syto 9 (free entry into all cells) and PI (entry only into membrane-permeabilized cells) by cells in the presence of peptides revealed the status of pore formation and closure more clearly. As shown (Figure 4), the Um-treated cells were permeable to Syto 9 (green) but not to PI (red), suggesting the inability of this peptide to permeabilize cells. In contrast, both Fm- and ΔFm-treated cells were PI permeable at 150 min but lost this ability at 18 h, suggesting pore closure. Thus, FACS, SEM, and fluorescence microscopy observations suggested that a concentration- and time-dependent phenomenon involving peptide oligomerization may lead to enhanced peptide uptake regulating the removal of ΔFm and Fm from

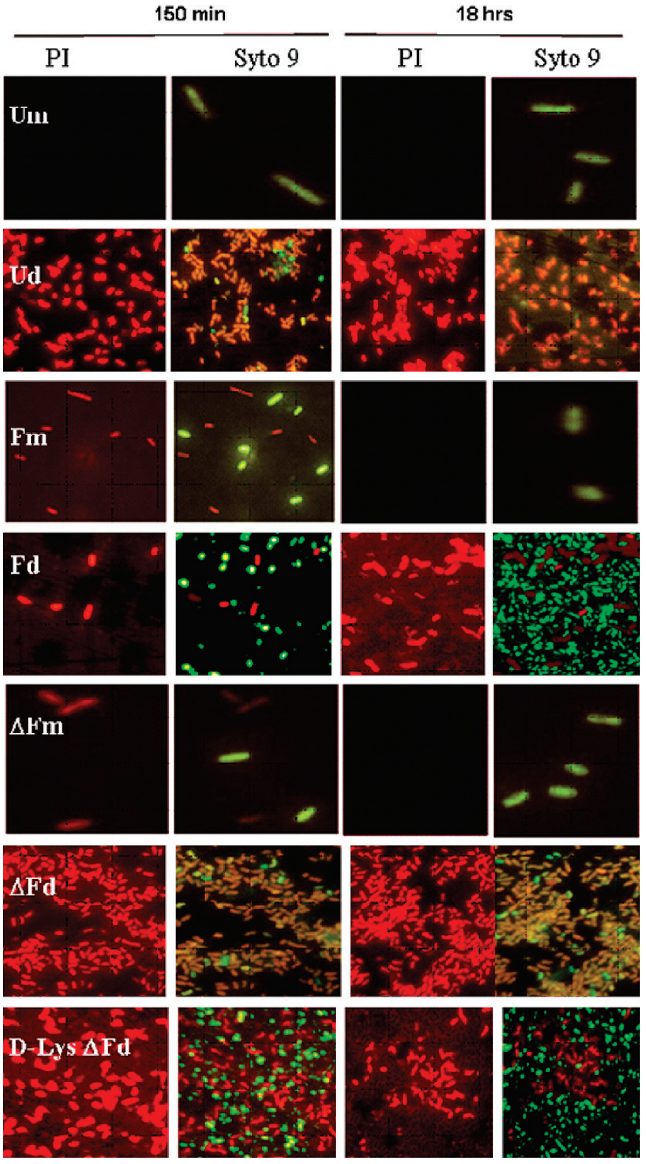

FIGURE 4: Fluorescence microscopy of peptide-induced permeabilization of *E. coli* ML35p cells visualized by PI and Syto 9 staining at 150 min and 18 h, respectively: Fm, ΔFm, and Um at 110 μM each, Fd at 3 μM, ΔFd at 2.5 μM, Ud at 30 μM, and D-Lys-ΔFd at 5 μM. These concentrations represent the MICs of the respective peptides with the exception of those of Fm and Um.

the inner membrane of cells. In sharp distinction to the monomers Um (no permeabilization) and Fm and ΔFm (transient permeabilization), the PI uptake images with the corresponding dimers Ud, Fd, and ΔFd showed an "open pore" status of cells even after overnight incubation. Interestingly, the nonhelical dimer D-Lys-ΔFd also turned out to be a persistent permeabilizer.

RPHPLC Study of Translocation of Peptides to the Bacterial Cytosol. We have used the intrinsic absorbance (280 nm) of Fm, Um, and ΔFm to monitor the uptake and stability of peptides incubated with bacteria using RPHPLC. All these three peptides have a tryptophan each (ε_{280} = 5050 M^{-1} cm^{-1}). In addition, ΔFm has three strongly absorbing (ε_{280} = 19000 M^{-1} cm^{-1}) ΔF residues. As shown (Figure 5A), the maximum recoveries of Um and Fm were in the respective cell supernatants, while the supernatant of ΔFm-treated cells was free of any significant peak (panel Aii). It may be noted that unlike Um which showed a single major peak at the retention time of the parent peptide, the profile of the supernatant of Fm-treated cells

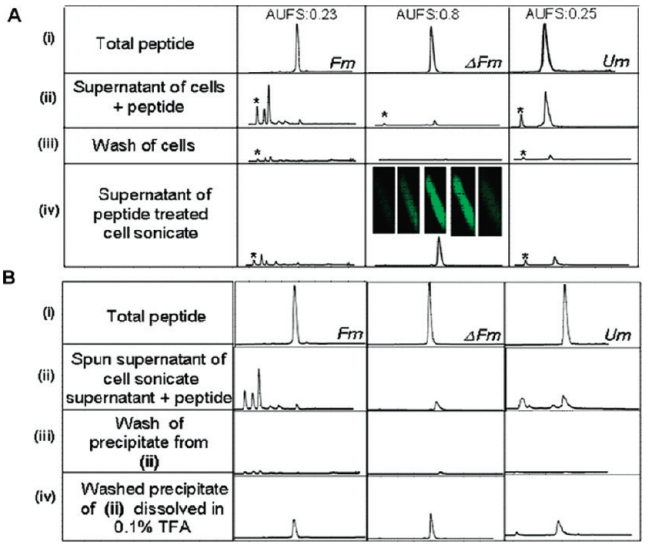

FIGURE 5: (A) RPHPLC study of uptake of peptides by *E. coli*. Samples obtained at different stages indicated as i–iv have been chromatographed (μ Bondapak C_{18} column, 4 μm, 3.9 mm × 300 mm, flow rate of 1 mL/min, gradient from 5 to 75% acetonitrile, 0.1% TFA in 70 min). The inset in panel Aiv shows the intracellular distribution of FITC-ΔFm as seen by confocal optical sectioning where the focal plane was changed from top (left) to bottom (right) in the vertical axis between 0 and 2 μm at an interval of 0.5 μm. The peaks marked with an asterisk appeared in cells alone without any peptide treatment. (B) RPHPLC analysis of interactions between peptides and cytosol incubated and processed as described in Experimental Procedures. Samples obtained at stages i–iv have been chromatographed as described for panel A. The abscissa and ordinate in both panels represent time (minutes) and absorbance (millivolts), respectively. All chromatograms were run under identical conditions and have been aligned on identical time axes.

showed a major peak and two minor peaks with retention times preceding the parent peptide. This suggests that Fm undergoes proteolytic degradation by *E. coli*. After the cells had been washed free of peptide and confirmation of washing by HPLC (panel Aiii), we sonicated them to look for the peptide that may have been translocated into the cells. The analysis of cell sonicate supernatants revealed that only ΔFm was present intracellularly in significant amounts (panel Aiv). To confirm that ΔFm was indeed cytosolic, we subjected *E. coli* cells incubated with FITC-labeled ΔFm to optical sectioning by confocal microscopy. As shown (Figure 5Aiv, inset in the ΔFm panel), the optical sections yielded negligible fluorescence at the periphery and strong fluorescence at the core, indicating a cytosolic location of ΔFm.

Comparative Proteolytic Stability of Fm, Um, and ΔFm in E. coli Cytosolic Extracts. In an attempt to determine the sensitivity of the three peptides (Fm, ΔFm, and Um) to possible degradation by proteases, we incubated each of them with bacterial cytosolic extract. However, the process of mixing peptide solutions with the cytosol elicited turbidity, giving pellets on centrifugation. The RPHPLC analyses of the three supernatants (Figure 5B) revealed that Fm was largely degraded; the pattern of RPHPLC peaks obtained from cytosolic extract-mediated degradation (Figure 5Bii) was a replica of the degradation pattern shown by intact *E. coli* (Figure 5Aii). The supernatant of the corresponding ΔFm sample gave a single minor peak at the same retention time as the parent peptide. The Um peptide supernatant exhibited three peaks preceding the peak of the parent peptide. However, the HPLC analysis of the pellets from the respective peptides and cytosol mixtures after dissolution in 0.1% TFA showed the presence of each of the three

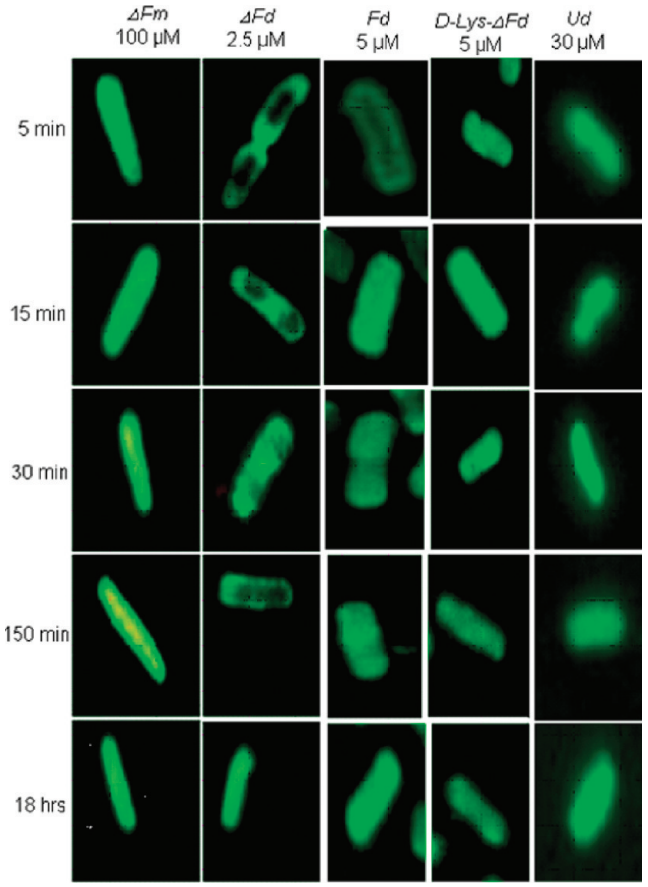

FIGURE 6: Fluorescence microscopic time kinetics of the uptake of FITC-tagged peptides by *E. coli* ML35p. Each peptide was studied at its MIC as indicated against the respective peptide. The experiment was conducted in 10 mM sodium phosphate buffer (pH 7.5) on log phase bacteria at an A_{600} of 0.4. Note the rapid translocation of ΔFm, the intermediate rate of transfer of Fd, and the slowest transfer of ΔFd. The other two dimers, viz. Ud and D-Lys-ΔFd, are also seen to translocate in the rapid mode resembling ΔFm.

peptides in its respective pellet. It may be noted that in a study of the comparative susceptibilities of Um, Fm, and ΔFm to the proteolytic actions of trypsin and chymotrypsin, we observed that ΔFm was more stable than Fm and Um to trypsin and ΔFm and Um were more stable than Fm to chymotrypsin (Figure 4 of the Supporting Information).

Translocation of FITC-Tagged AMPs into E. coli. To determine if subsequent to peptide-induced membrane permeabilization, the peptides would be translocated into cells, we incubated *E. coli* with the respective FITC conjugates to visualize these peptides in bacteria. A comparative time kinetics analysis of the cellular location of FITC-ΔFm versus FITC-ΔFd using fluorescence microscopy (Figure 6) indicated that the monomeric ΔFm is translocated from the membrane to the cytosol much faster than the dimeric ΔFd. Early at 5 min, while FITC-ΔFm appears to be intracellular, the dimeric FITC-ΔFd lags behind, exhibiting a predominantly membrane bound status. At later time points between 15 and 150 min, FITC-ΔFd continues to stay put at the membrane even as gradual and progressive translocation into the cytosol is apparent. At 18 h, the translocation of FITC-ΔFd into the cell appears to be complete. All other dimers, including Fd, Ud, and D-Lys-ΔFd, seem to translocate into the cell much faster than ΔFd.

Dimer ΔFd Is More Trypsin Resistant Than Monomer ΔFm and Dimers Fd and Ud. Proteolytic vulnerability of

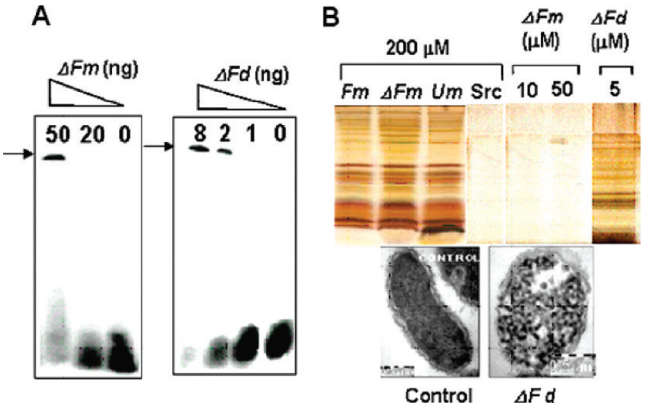

FIGURE 7: Comparative potencies of dimeric ΔFd vs monomeric ΔFm antimicrobial peptides for DNA gel retardation and bacterial cytosolic protein precipitation. (A) Polyacrylamide gel electrophoresis-based DNA gel retardation assay. A P^{32}-end-labeled 16mer double-stranded DNA probe has been used. The arrow indicates retarded DNA. (B) Silver-stained SDS−PAGE analysis of precipitation of cytosolic proteins of *E. coli* by peptides (top). The spun pellets of cytosol and peptide have been loaded. TEM images of untreated control and 2.5 μM ΔFd-treated *E. coli* (bottom).

peptides is governed not only by residue characteristics but also by peptidomimetic design elements. Thus, it has been reported that branched dendrimeric peptides exhibit greater biochemical stability over their monomeric counterpart (*33*). Indeed, when we examined the comparative stabilities of the monomer ΔFm versus the dimer ΔFd to trypsin, we found the dimer to be far more stable than the monomer (Figure 5 of the Supporting Information). A comparison of the relative trypsin stabilities of the four dimers (Fd, Ud, ΔFd, and D-Lys-ΔFd) (Figure 6 of the Supporting Information) indicated that Ud and Fd were relatively more susceptible to proteolysis, ΔFd showed considerably greater stability, and as expected D-Lys-ΔFd was the most stable.

Dimer ΔFd Is More Potent Than Monomer ΔFm in DNA Gel Retardation and Precipitation of Cytosolic Proteins. The features of cationic character in an amphipathic helix, which are known to facilitate the interactions of AMPs with bacterial membranes, could in principle also allow optimal interactions of AMPs with nucleic acids. As shown in Figure 7A, both ΔFm and ΔFd exhibited effective gel retardation of radiolabeled DNA. However, while the effective amount for causing gel retardation was between 20 and 50 ng for monomeric ΔFm, dimeric ΔFd exhibited potent gel retardation at the low dose of 2 ng. Since we had observed formation of precipitates on mixing *E. coli* cytosol fraction with monomeric cationic peptides (Fm, ΔFm, and Um), we set out to determine what was being precipitated by these peptides. When the precipitates were subjected to SDS−PAGE analysis (Figure 7B), it became evident that the three monomeric peptides (Fm, ΔFm, and Um) at 200 μM were indeed causing the precipitation of a large number of cytosolic proteins. In contrast, several other peptides, including Src, NS4, and oxytocin, also tested at 200 μM failed to show any precipitation. We then evaluated the potency of protein precipitation by monomer ΔFm versus dimer ΔFd. As shown, while ΔFd showed protein precipitation at 5 μM (its MBC against *E. coli*), ΔFm failed to show any protein precipitation up to a concentration of 50 μM. It was interesting to note that TEM images of ΔFd-treated *E. coli* (Figure7B, bottom panel) also had numerous flocculation bodies.

Aromatic Dimers Fd and ΔFd Are the Fastest in Killing E. coli. The kill kinetics data (Figure 8) demonstrate the rapid

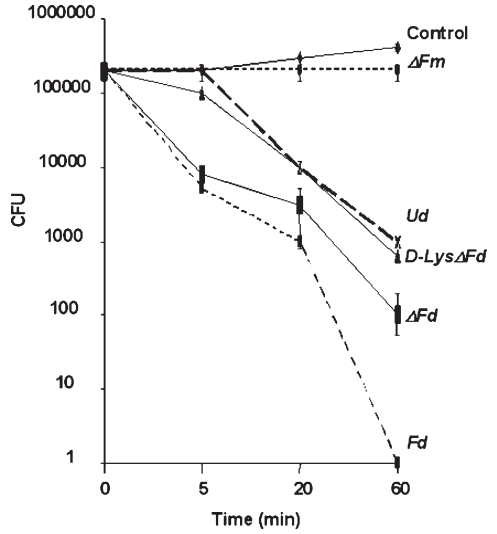

FIGURE 8: Kill kinetics of *E. coli* ML35p by ΔFm, ΔFd, Fd, D-Lys-ΔFd, and Ud each at 4 times its MIC. Samples withdrawn at the indicated times were evaluated for colony forming units. ΔFd and Fd kill ~97% of the cells within the first 5 min.

action of Fd and ΔFd which kill 97% of the cells within the first 5 min. By 20 min, Fd shows killing of ~99% of the cells while ΔFd seems to become a little slower, killing ~98% of the cells. In contrast, Ud and D-Lys-ΔFd show no killing in the first 5 min followed by killing of ~95% of the cells at 20 min.

DISCUSSION

A credible understanding of the mechanisms of drug action can aid faster evolution of better drugs. The driving force of our studies was to investigate the finer details of the action of de novo designed antibiotic peptides. As targets of antibiotic peptide action, bacteria seem to present a combination of primordial simplicity and evolved sophistication. Thus, binding studies with a variety of de novo designed peptides indicated that the degree of cationic charge on a peptide determines its binding affinity for LPS (Figure 2A). It may be recalled that LPS, which forms an effective permeability barrier, plays a major role in the resistance of Gram-negative bacteria toward toxic agents. However, the immediate downstream effect of LPS binding viz. the outer membrane permeabilization appears to be peptide specific and not linked to a simple feature like charge density. Thus, within the triplet of isocharge (+3) peptides (Fm, ΔFm, and Um), only the first two densely aromatic peptides caused outer membrane permeabilization (Figure 2B). The inability of Um to cause membrane permeabilization indicates the seminal role of aromatic residues in destabilizing the membrane. In general, a tendency for aromatic amino acids to occur in the membrane interface has been noted (*34*). It seems that such tendencies of lipid peptide interactions may be responsible for the marked distinctions in the observed permeabilization abilities of the largely aliphatic Um versus the highly aromatic Fm or ΔFm. It is interesting to note that biocides like Phenol and quaternary ammonium compounds were in use at the beginning of the 20th Century when there were few drugs for treatment of infections (*35*). The nonspecific action of such biocides restricts their utility only for external applications. In contrast, the virtue in the cationic−aromatic AMPs like Fm and ΔFm is the ability of positive charges to target the phenyl or indole moieties specifically to bacteria.

The peptide concentration−PI permeabilization relation (Figure 3) was linear for Fm but inverse for ΔFm. While the exact cause for this inverse relationship exhibited by ΔFm is unclear, the differential biochemical stabilities of Fm versus ΔFm in *E. coli* (Figure 5) may provide an explanation. The equilibrium between oligomeric and monomeric Fm is likely to be influenced by proteolysis such that oligomers may give rise to monomers not allowing a build up of the critical threshold concentration of oligomeric assembly required for translocation. In contrast, the greater biochemical stability of ΔFm (Figure 4 of the Supporting Information) coupled with a strong tendency of ΔF-containing peptides to oligomerize (*15*, *25*) may indeed allow the formation of oligomeric assemblies of the critical threshold size that may trigger "spontaneous" peptide translocation into the cytosol. This may explain why Fm exhibits an increased level of permeabilization at 100 μM versus that at 50 μM while ΔFm exhibits a reduced level of permeabilization at 100 μM versus that at 50 μM.

In comparison to monomer ΔFm, dimer ΔFd was distinctly more potent in permeabilizing bacterial membranes (Figures 2 and 3). In recent studies, a large increase in pore forming ability has been observed with multivalent magainin compounds (*14*). It is worth remembering that inherent to dendrimer design are the features of an increased effective molarity of monomeric units and a decrease in the entropy of self-assembly (*12*). In addition, the ability of ΔF residues to facilitate both inter- and intramolecular long-range interactions is well-documented (*15*, *25*). Thus, a stable bivalent state in ΔFd coupled with the "sticky" characteristic of ΔF can indeed nucleate large oligomeric states leading to a high degree of membrane permeabilization at fairly low concentrations of this peptide.

A large number of naturally occurring AMPs, including cecropins, mellitin, and magainin, that are well-known to form pores in biomembranes are cationic, amphipathic α-helical peptides. Such a conformation is thought to facilitate efficient interaction of these peptides with biomembranes (*10*). Ours is the first report of the use of ΔF in de novo design of a potent 3_{10}-helical dimeric AMP. This antimicrobial represents the coming together of cationic character in an amphipathic, helical fold on a dimeric scaffold. The significance of helicity in enhancing antibiotic potency is evident from the low potency of the analogously designed nonhelical dimeric isomer, viz. D-Lys-ΔFd, which shares almost all properties of ΔFd except that it is not helical. It is interesting to see (Table 3) that ΔFd with an MBC/MIC ratio of 5/2.5 = 2 is by definition bactericidal against *E. coli*. In contrast, a high MBC/MIC ratio of 25/5 = 5 for D-Lys-ΔFd suggests it to be less of a bactericide and more of a bacteriostat. Applying conventional definitions based on the MBC/MIC ratio, both ΔFd (MBC/MIC ratio of 7.5/5 = 1.5) and D-Lys-ΔFd (MBC/MIC ratio of 150/55 = 2.7) appear to be bactericidal against *S. aureus*. However, the significantly low potency of D-Lys-ΔFd would nevertheless make it a poor antibiotic. It may be noted that bactericidal drugs are preferred over bacteriostatic drugs in antibiotic therapy since the former curtail the emergence of antibiotic resistant bacteria (*36*). A comparison of the increments in MIC in going from ΔFd to D-Lys-ΔFd (Table 3) indicates that it is 2-fold for *E. coli* but 11-fold for *S. aureus*. Likewise, the corresponding increment in MBC is 5-fold for *E. coli* and 20-fold for *S. aureus*. This suggests that the requirements of helicity for stalling growth or causing bacterial death may be much stronger for Gram-positive bacteria than for Gram-negative bacteria. The underlying structural reasons for this phenomenon need to be more deeply investigated.

In its antimicrobial targeting strategy, dimer ΔFd appears to be qualitatively distinct from monomer ΔFm. As shown

(Figure 4), early at 150 min, both ΔFm and ΔFd permeabilized cells to PI. However, following overnight incubation, while the ΔFm-treated cells were no longer permeable, the ΔFd-treated cells continued to remain permeable to PI. This suggests that the pores formed by ΔFm are transient which close following entry of the peptide into the cells. In contrast, the persistent permeability seen in ΔFd-treated cells indicates that the dimeric pores have a much longer residence time on the membrane. This indicates that a bivalent structure such as the dimer by virtue of strong binding of an amphipathic positively charged peptide helix might retard the translocation of the peptide into the cell. However, this does not mean that the cells do not take up ΔFd. Indeed, as shown (Figure 6), the FITC-labeled derivatives of both ΔFm and ΔFd appear to be taken up by bacteria. However, examination of the cellular location of the dimer as a function of time revealed that it is predominantly membrane-anchored at an early time point (5 min), followed by membrane cum cytosol dual localization at intermediate time points (15, 30, and 150 min) and a largely cytosolic localization at 18 h. A strongly permeable status (Figure 4) associated with predominantly cytosolic localization (Figure 6) of the dimer at 18 h indicates the lack of a strong correlation between the presence of the peptide on the membrane and membrane permeabilization. A closer look at the data suggests that the phenomenon of membrane permeabilization [PI + at 150 min (Figure 4)] subsequent to peptide translocation [cytosolic location at 5 min (Figure 6)] is seen for a shorter time window also for ΔFm. Indeed, a more precise determination of the time of closure of pores formed by ΔFm (Figure 7 of the Supporting Information) indicated that the cells became PI impermeable only at around 4−5 h even as this peptide was intracellular as early as 5 min. In light of these observations, models of membrane permeabilization may include the possibility of peptide-induced membrane damage, which cannot be instantly revoked by peptide translocation. In essence, our data suggest that even as both monomer ΔFm and dimer ΔFd permeabilize the membrane and translocate themselves into the cytosol, the cell remains PI permeable even in the apparent absence of the peptide on the cell surface. However, the imprint of the permeabilized status of the membrane persists for a shorter duration (4−5 h) for monomer ΔFm than is the case with dimer ΔFd (up to 18 h).

It is interesting to note that many biochemical parameters monitored in response to antibiotic action in this study seem to be reliable correlates of antibiotic potency. Thus, in several cases including outer (Figure 2B) and inner (Figure 3) membrane permeabilizations, cytosolic protein precipitation (Figure 7B), and DNA gel retardation (Figure 7A), the observed phenomena were seen for individual peptides at concentrations in the vicinity of their respective MICs. Likewise, in studies conducted at MICs of different peptides, the direct correlation between peptide-induced membrane permeabilization as studied by FACS and SEM (Figure 3) suggests that FACS may have predictive value for the changes seen at the bacterial surface.

The field of AMPs is divided between those that believe in membrane permeabilization as the primary target of action and the others who postulate that bacteria are not severely affected by momentary leakiness of the membrane and that these peptides kill by perturbing intracellular targets (*10*). Indeed, membrane integrity is vital to all living things for the maintenance of transmembrane ionic gradients that govern fundamental cellular processes like oxidative phosphorylation-mediated biosynthesis of ATP. Similarly, many intracellular targets of AMP action, e.g., inhibition of replication, transcription, and translation, are now known (*10*). We believe that AMPs may indeed target bacteria from the periphery as well as the interior of the cell. In this context, the case of Fm versus ΔFm is interesting. These two are equipotent at membrane permeabilization (Figures 2 and 3), but only ΔFm exhibited modest antibiotic action (Table 2). The probable reason for this edge in ΔFm over Fm may lie in the ability of ΔFm to enter the cell (Figure 6) and perturb intracellular targets. It is worth noting that the membrane permeabilizing effect of Fm is sufficient to paralyze bacterial biochemistry leading to a state of cytostasis (Figure 2C). However, following the digestion of Fm by bacterial proteases (Figure 5), the cells recover from cystostasis and soon resume good growth. In contrast, ΔFm seems to first confer a cytostasis effect via membrane permeabilization, and soon thereafter, it invades cells to perturb the intracellular milieu. Such a coordinated action both at the membrane and in the cytosol seems to make ΔFm a persistent and potent cytostatic AMP (Figure 2C). Nevertheless, an MBC/MIC ratio of 4.5 (Table 2) suggests that ΔFm is not bactericidal. A glimpse of the vital roles of both membrane and intracellular targets of AMP action is illustrated by the 100-fold higher antibiotic potency of ΔFd over ΔFm (Table 2). The features associated with the modestly antibiotic ΔFm include (a) a milder degree of membrane permeabilization (Figures 2B, 3, and 4), (b) rapid peptide translocation (Figure 6), and (c) a rather short period (~4 h) (Figure 7 of the Supporting Information) of PI permeability. Against this, the hallmarks of the strongly antibiotic ΔFd include (a) strong membrane permeabilization (Figures 2B, 3, and 4), (b) physical association of the peptide with the membrane at least up to 150 min (Figure 6), and (c) a prolonged period (up to 18 h) (Figure 4) of PI permeability. Membrane permeabilization and entry of peptide into the cell appear to be sequential events in the case of ΔFm. However, these two events appear to be concurrent in the case of ΔFd, which shows protracted membrane permeabilization (Figure 4) even as substantial amounts also find their way into the cell cytosol (Figure 6). Once inside the cell, ΔFm and ΔFd seem to cause precipitation of cytosolic proteins, and TEM of ΔFd-treated cells indeed shows distinct dense precipitation bodies (Figure 7B). Such precipitation is most probably a consequence of both the strong aromaticity and the strongly basic character inherent in ΔFm and ΔFd. Interestingly, similar flocculation bodies have also been observed in the action of anionic AMPs (*37*). However, since bacterial proteins are, on average, more acidic than the proteins of eukaryotes (*38*), it is suggested that cationic AMPs may have an edge over anionic AMPs in causing flocculation of intracellular bacterial proteins. Gel retardation experiments (Figure 7A) suggest that nucleic acids may also be the targets of ΔFm and ΔFd. In targeting bacteria, the dimer is 7-fold more potent than the monomer also because the bivalency and the associated avidity inherent to the dimer enhance its potency for DNA gel retardation and protein precipitation (Figure 7). The combined consequences of membrane permeabilization, intracellular protein precipitation, and binding to nucleic acids can indeed be disastrous, leading to fast inhibition of bacterial growth (ΔFm) or bacterial death (ΔFd).

A major drawback with the use of peptide drugs is their degradation by proteolytic enzymes. The arginine- and lysine-derived cationic character inherent to most antimicrobial peptides also renders them vulnerable to degradation by serine proteases like trypsin. While the S1 site in trypsin is responsible for binding to Lys or Arg in the substrate, the S2 site plays a role

in catalyzing the hydrolysis of the peptide bond carboxy-terminal to lysine or arginine. In a recent study, Svenson *et al.* using docking studies showed that rigid lipophilic bulky side chains of residues on the C-terminus of Arg sterically hindered binding of the substrate to the S2 site (*39*). It may be noted that α,*β*-didehydrophenylalanine has a conformationally rigid, planar, lipophilic bulky side chain that may confer resistance to trypsin by this mechanism. This is evident from the observation that ΔFm was more stable to trypsin compared to Fm or Um (Figure 4A of the Supporting Information). Second, it is well-known that many potential protease cleavage sites in folded proteins remain undigested while the same are digested with ease in the fully unfolded proteins. The reason for this selective protection could be the inaccessibility of several scissile peptide bonds in the folded protein. In support of this hypothesis, synthetically created all-hydrocarbon cross-linkers have been found to confer metabolic stability to peptides through enhancement of peptide helicity (*40*). The comparative stability of ΔFm vis-à-vis Fm against trypsin is likely to be influenced by (a) the tendency of ΔFm to assume a helical structure in the environment of the bacterial membrane and (b) the inhibitory influence of the didehydrophenylalanine residue at the S2 site as discussed above. The fact that dimer ΔFd is more stable than ΔFm against trypsin is likely to be due to the dimer design which confers greater conformational stability to peptide chains when they are proximal as in a branched dimer (e.g., ΔFd) than when they are isolated (e.g., ΔFm). In contrast to the rapid degradation of Fm (Figure 4B of the Supporting Information), the relative stability of ΔFm against chymotrypsin (a protease that cleaves the peptide bond carboxy-terminal to Phe, Tyr, and Trp) suggests the inability of chymotrypsin to digest ΔF-X peptide bonds. This is consistent with the fact that neither the peptide bond nor the side chain characteristics in ΔF-X bear any resemblance to those of F-X. The peptide bond in ΔF-X would be conformationally constrained, while the same in F-X would be more relaxed. Likewise, while the side chain aromatic ring in ΔF-X, because of the double bond from Cα to C*β* in ΔF, would be planar and rigid, the corresponding side chain in F-X would be tetrahedral and freely rotating. Stabilization against proteases is of great significance to peptide drugs in general and antimicrobial peptides in particular. Different degrees of stabilization of AMPs against proteases are likely to influence important mechanistic parameters like (a) the increased stability of oligomeric peptide assemblies on the bacterial membrane leading to sustained and potent permeabilization and (b) the increased intensity of intracellular targeting. These parameters in turn have a direct bearing on antimicrobial peptide potentiation as seen in moving from Fm (most unstable to trypsin, MIC of >500 μM) to ΔFm (intermediate stability to trypsin, MIC of 100 μM) to ΔFd (most stable to trypsin, MIC of 2.5 μM).

The significant enhancement in antibacterial potency observed following dimerization of ΔFm prompted us to investigate if similar dimerization of Fm and Um may also enhance the potency of these inactive peptides. Although dimerization resulted in significant improvement in the antibiotic potency of all monomers studied by us (Tables 2 and 3), no two dimers were alike in their traits. Thus, Ud suffered from high MIC and MBC values against *E. coli* and no action against *S. aureus*; Fd was quite potent against *E. coli* but had no promise against *S. aureus*, and D-Lys-ΔFd showed a low-MIC−high-MBC combination against *E. coli* with poor activity against *S. aureus*. Relative protease stability experiments using trypsin indicated that the nonhelical dimer (D-Lys-ΔFd) was the most stable and helical dimer ΔFd was a close second. However, both Ud and Fd were found to be quite labile to proteolysis. Our data suggest that each dimer was competent in causing persistent membrane permeabilization (Figure 4) and self-penetration (Figure 6) into *E. coli*. The nearly equal potencies of ΔFd and Fd and the rather low activity of Ud against *E. coli* suggest the importance of aromatic residues in an amphipathic, cationic peptide for action against *E. coli*. It may be recalled that in its monomeric state, ΔFm is moderately potent against *E. coli* and almost inactive against *S. aureus*, while Fm and Um are inactive against both *E. coli* and *S. aureus*. Dimerization was found to potentiate the antimicrobial action of not only ΔFm but also Fm to approximately similar MIC values of 2.5 and 3.0 μM, respectively, against *E. coli*. However, the increase in potency against *S. aureus* was significantly different with MICs of 5 μM (for ΔFd) and 45 μM (for Fd). These data (Table 3) seem to suggest a predominant effect of dimerization on the potentiation seen with these two aromatic peptides against both the Gram-negative *E. coli* and the Gram-positive *S. aureus*. It is worth emphasizing that the ratio of *S. aureus* to *E. coli* MICs for ΔFd is $5/2.5 = 2$, while the same ratio for Fd is $45/3 = 15$. As ΔFd would be a stronger helix (because of the conformational rigidity of ΔF) than Fd, these data point to more stringent requirements of helical structure for effective antibiotic action against the Gram-positive *S. aureus* than against the Gram-negative *E. coli*. This phenomenon is corroborated also by the fact that the nonhelical dimeric analogue of ΔFd, viz. D-Lys-ΔFd, also exhibited a high value of 11 for this ratio. These results confirm a previous finding suggesting a more stringent requirement of helical structure in AMPs targeting Gram-positive bacteria than in those that target Gram-negative bacteria (*8*). It is noteworthy that dimer D-Lys-ΔFd exhibited a combination of low MIC and high MBC against *E. coli* and was quite inactive against *S. aureus*. It therefore suggests that aromatic cationic character may be sufficient to inhibit the growth of *E. coli*, but these features must be embedded in a helical fold for effective killing of not only *S. aureus* but also *E. coli*. The potentiation effect seen in the case of Ud (the dimer, *E. coli* MIC of 30 μM) is quite remarkable considering the inability of Um (the monomer, *E. coli* MIC of >500 μM) to either permeabilize (Figure 4) or penetrate (data not shown) *E. coli*. On probing into the doings of Ud that made it become substantially potent, we observed the advent of two features, viz. the ability to permeabilize (Figure 4) and the ability to penetrate (Figure 6) cells. It may be noted that while Um is monomeric and largely aliphatic (one tryptophan residue), dimer Ud has two tryptophan residues. The combination of these two features in Ud seems to potentiate its permeabilization ability significantly, resulting in a mild antibiotic effect against *E. coli*.

Since our results suggested that dimerization may be a generic motif that potentiates antimicrobial action, it was pertinent to compare the potency and spectrum of action of lysine branched dimer ΔFd with those of linearly dimerized analogue $(\Delta Fm)_2$. As shown (Table 2), in targeting *E. coli*, linear dimer $(\Delta Fm)_2$ was indeed equipotent with branched dimer ΔFd. However, against *S. aureus*, the branched dimer was 4-fold more potent than the linear dimer. A comparison of the helical propensities of ΔFd versus $(\Delta Fm)_2$ (Figure 1C) indicates that even as these two dimers are nearly identical in sequence, amino acid composition, and molecular mass, the branched dimer is a significantly stronger helix than the linear dimer. The three dimeric peptides, ΔFd, $(\Delta Fm)_2$, and D-Lys-ΔFd, share almost all features (Table 1)

except that ΔFd is highly helical, $(\Delta Fm)_2$ is moderately helical, and D-Lys-ΔFd is nonhelical (Figure 1C). The antimicrobial potencies of these three peptides (Figure 9) indicate the redundancy of helical structure for action against *E. coli* and the strong requirement of the same for action against *S. aureus*. The high value of the ratio of the MIC for *S. aureus* to the MIC for *E. coli* (Table 3) seen in cases of D-Lys-ΔFd (nonhelical) and $(\Delta Fm)_2$ (weakly helical) suggests that while *E. coli* can be challenged by weakly helical dimeric AMPs, only a strongly helical dimeric AMP like ΔFd is competent to target *S. aureus*.

Our data suggest that dimer ΔFd works so well against both Gram-negative *E. coli* and Gram-positive *S. aureus* because of the assembly of a large number of positive attributes in a single molecule. These include (a) strong, amphipathic helicity nucleated by the planar aromatic didehydrophenylalanine residues, (b) the dimeric design which augments the avidity of the molecule for bacterial molecular motifs like the LPS in Gram-negative bacteria and the teichoic acids (*41*) in Gram-positive bacteria, (c) the dimeric design which augments the avidity of the molecule for DNA and proteins intracellularly, and (d) the dimeric design which augments the avidity of the cell surface molecular interactions that lead to heightened membrane permeabilization. It is worth noting that the planar ΔF residue has strong tendencies to engage in long-range weak CH···O hydrogen bonds, which allowed us to assemble the first de novo designed helical hairpin peptides (*15*, *23*). This feature is capable of facilitating the formation of large oligomeric peptide channels dissipating membrane potential. However, our data suggest that the single most important reason that this dimeric design is so potent against both Gram-negative and Gram-positive bacteria may be the subtle but seminal difference in the kinetics of entry of dimers Ud and D-Lys-ΔFd on the one hand and ΔFd and Fd on the other. While the former two are translocated into bacteria very fast (Figure 6), Fd (in a small measure) and ΔFd (in a large measure) show the tendency for a longer residence time on the cell surface. This allows dimer ΔFd and to a lesser extent also dimer Fd to target both the surface and the cell interior simultaneously and aggressively. The synergy created by this simultaneous action is the one that may be instrumental in facilitating the potent killing of both Gram-negative and Gram-positive bacteria by ΔFd and the potent killing of *E. coli* alone by Fd. The reason for faster killing of *E. coli* by Fd and ΔFd than all the other dimers (Figure 8) may also originate from the acceleration of events leading to cell death when challenged from both inside and outside simultaneously.

A high specificity for targeting bacteria coupled with widespread binding to intracellular proteins and nucleic acids may enable ΔFd to function as a "smart" drug. These unique properties of ΔFd can spur the design of a repertoire of novel molecules that bacteria may find hard to challenge. The time window of

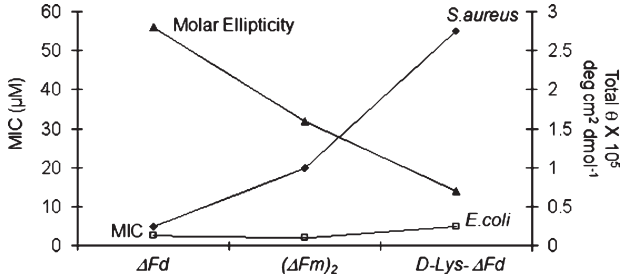

FIGURE 9: Helicity is more crucial for antimicrobial action against *S. aureus* than against *E. coli*. The three dimeric peptides, ΔFd, $(\Delta Fm)_2$, and D-Lys-ΔFd. share almost all features (Table 1) except that ΔFd (lysine-branched dimer) is highly helical, $(\Delta Fm)_2$ (linear dimer) is moderately helical, and D-Lys-ΔFd (lysine-branched dimer with D-lysines as helix terminators) is nonhelical. The inverse correlation between helicity and MIC is marginal for *E. coli* but sharply pronounced for *S. aureus*. The molar ellipticity data shown are for the intensity of the 267 nm CD band shown in Figure 1C.

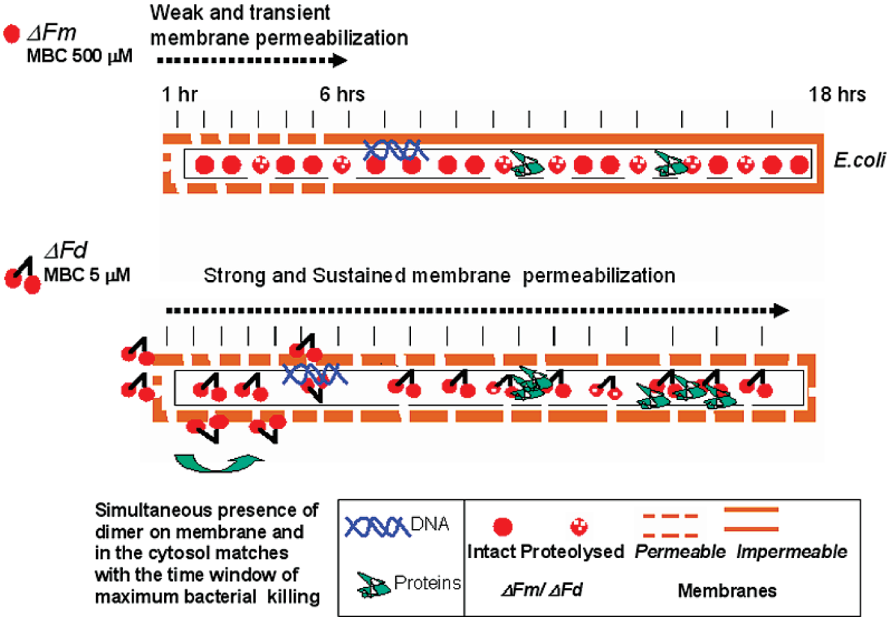

FIGURE 10: Model indicating the likely mechanism for the 100-fold higher antibacterial potency of dimer ΔFd (MBC of 5 μM) over monomer ΔFm (MBC of 500 μM) against *E. coli*. The dimer scores over the monomer in (a) having a longer residence time on the cell membrane, (b) causing sustained membrane permeabilization, (c) having a superior stability against proteases, and (d) having a stronger avidity (by virtue of its bivalent character) for binding to intracellular proteins and nucleic acids. Most significantly, the time window (green arrow) when the dimer is both on the cell surface and inside the cytosol coincides with the time period when maximum bacterial death is observed. This suggests that the synergy of simultaneous and potent action from both the surface and inside the cell, unique to the dimer and absent in the monomer, may be instrumental in the 2 order of magnitude antibiotic potentiation seen in the dimer over the monomer. This feature may also explain why the dimer is broad spectrum in action, acting against both the Gram-negative *E. coli* and the Gram-positive *S. aureus*.

15 min when ΔFd is seen both at the cell membrane and in the cytosol (Figure 6) is quite close to the time this peptide takes to kill ~98% of the cells (Figure 8). A model illustrating the characteristic distinctions in the manner in which *E. coli* responds to monomer ΔFm versus dimer ΔFd is shown in Figure 10. The propensity of antimicrobial peptides to target both the cell surface and the cytoplasm may indeed confer an evolutionary advantage on these ancient sentinels of innate immunity.

ACKNOWLEDGMENT

Gifts of *E. coli* ML35p from Dr. Liam Good (Karolinska Institutet, Stockholm, Sweden) and *S. aureus* ATCC 700699 from Dr. R. P. Roy (NII, New Delhi, India) are gratefully acknowledged. The assistance of Dinesh and Yasmeen [antimicrobial action of $(\Delta Fm)_2$], Dr. S. Reddy [mass spectrum of $(\Delta Fm)_2$], and Naveen [CD spectrum of $(\Delta Fm)_2$] is acknowledged. We thank Dr. Raj Bhatnagar (ICGEB, New Delhi, India) for his keen interest in our research and Dr. R. P. Roy for his valuable input on the manuscript. Finally, we thank all the anonymous reviewers whose insightful comments have provided immense strength to the manuscript.

SUPPORTING INFORMATION AVAILABLE

Experimental procedures for synthesis, FITC labeling, and purification of peptides; circular dichroism spectra for monomeric peptides (Figure 1); hemolytic activity of branched dimers (Figure 2); salt tolerance of monomer versus dimer (Figure 3); comparative stabilities of monomeric peptides to trypsin and chymotrypsin (Figure 4); comparative stabilities of monomer versus dimer to trypsin (Figure 5); comparative stability of branched dimers to trypsin (Figure 6); kinetics of pore formation and closure in *E. coli* treated with ΔFm (Figure 7); and mass spectroscopic characterization of monomeric (Figure 8), branched dimeric (Figure 9), linear dimeric (Figure 10), FITC-tagged ΔFm, Um, ΔFd (Figure 11), and FITC-tagged D-Lys-ΔFd, and Ud (Figure 12) peptides. This material is available free of charge via the Internet at http://pubs.acs.org.

REFERENCES

1. Tomasz, A. (2006) Microbiology: Weapons of microbial drug resistance abound in soil flora. *Science 311*, 342–343.
2. D'Costa, V. M., McGrann, K. M., Hughes, D. W., and Wright, G. D. (2006) Sampling the antibiotic resistome. *Science 311*, 374–377.
3. Bulet, P., Stocklin, R., and Menin, L. (2004) Anti-microbial peptides: From invertebrates to vertebrates. *Immunol. Rev. 198*, 169–184.
4. Hancock, R. E., and Sahl, H. G. (2006) Antimicrobial and host-defense peptides as new anti-infective therapeutic strategies. *Nat. Biotechnol. 24*, 1551–1557.
5. Ahmad, A., Yadav, S. P., Asthana, N., Mitra, K., Srivastava, S. P., and Ghosh, J. K. (2006) Utilization of an amphipathic leucine zipper sequence to design antibacterial peptides with simultaneous modulation of toxic activity against human red blood cells. *J. Biol. Chem. 281*, 22029–22038.
6. Hilpert, K., Volkmer-Engert, R., Walter, T., and Hancock, R. E. (2005) High-throughput generation of small antibacterial peptides with improved activity. *Nat. Biotechnol. 23*, 1008–1012.
7. Fernandez-Lopez, S., Kim, H. S., Choi, E. C., Delgado, M., Granja, J. R., Khasanov, A., Kraehenbuehl, K., Long, G., Weinberger, D. A., Wilcoxen, K. M., and Ghadiri, M. R. (2001) Antibacterial agents based on the cyclic D,L-α-peptide architecture. *Nature 412*, 452–455.
8. Giangaspero, A., Sandri, L., and Tossi, A. (2001) Amphipathic α helical antimicrobial peptides. A systematic study of the effects of structural and physical properties on biological activity. *Eur. J. Biochem. 268*, 5589–5600.
9. Peschel, A. (2002) How do bacteria resist human antimicrobial peptides?. *Trends Microbiol. 10*, 179–186.
10. Brogden, K. A. (2005) Antimicrobial peptides: Pore formers or metabolic inhibitors in bacteria?. *Nat. Rev. Microbiol. 3*, 238–250.
11. McAuliffe, O., Ross, R. P., and Hill, C. (2001) Lantibiotics: Structure, biosynthesis and mode of action. *FEMS Microbiol. Rev. 25*, 285–308.
12. Tam, J. P., Lu, Y. A., and Yang, J. L. (2002) Antimicrobial dendrimeric peptides. *Eur. J. Biochem. 269*, 923–932.
13. Liu, Z., Deshazer, H., Rice, A. J., Chen, K., Zhou, C., and Kallenbach, N. R. (2006) Multivalent antimicrobial peptides from a reactive polymer scaffold. *J. Med. Chem. 49* (12), 3436–3439.
14. Arnusch, C. J., Branderhorst, H., De Kruijff, B., Liskamp, R. M. J., Breukink, E., and Pieters, R. J. (2007) Enhanced membrane pore information by multimeric/oligomeric antimicrobial peptides. *Biochemistry 46*, 13437–13442.
15. Ramagopal, U. A., Ramakumar, S., Sahal, D., and Chauhan, V. S. (2001) *De novo* design and characterization of an apolar helical hairpin peptide at atomic resolution: Compaction mediated by weak interactions. *Proc. Natl. Acad. Sci. U.S.A. 98*, 870–874.
16. Kaiser, E., Colescott, R. L., Bossinger, C. D., and Cook, P. I. (1970) Color Test for Detection of Free Terminal Amino Groups in the Solid-Phase Synthesis of Peptides. *Anal. Biochem. 34*, 595–598.
17. Steinberg, D. A., Hurst, M. A., Fujii, C. A., Kung, A. H. C., Ho, J. F., Cheng, F. C., Loury, D. J., and Fiddes, J. C. (1997) Protegrin-1: A broad-spectrum, rapidly microbicidal peptide with in vivo activity. *Antimicrob. Agents Chemother. 41*, 1738–1742.
18. Manhong, W., and Hancock, R. E. W. (1999) Interaction of the Cyclic Antimicrobial Cationic Peptide Bactenecin with the Outer and Cytoplasmic Membrane. *J. Biol. Chem. 274*, 29–35.
19. Shin, S. Y., Kang, J. H., and Hahm, K. S. (1999) Structure-antibacterial, antitumor and hemolytic activity relationships of cecropin A-magainin 2 and cecropin A-melittin hybrid peptides. *J. Pept. Res. 53*, 82–90.
20. Hancock, R. E. W., Farmer, S. W., Li, Z., and Poole, K. (1991) Interaction of aminoglycosides with the outer membranes and purified lipopolysaccharide and OmpF porin of *Escherichia coli*. *Antimicrob. Agents Chemother. 35*, 1309–1314.
21. Hayat, M. A. (1981) Principle and Techniques of Electron Microscopy: Biological Applications , Edward Arnold, London.
22. Mosmann, T. (1983) Rapid colorimetic assay for cellular growth and survival: Application to proliferation and cytotoxicity assays. *J. Immunol. Methods 65*, 33–55.
23. Venkatraman, J., Shankaramma, S. C., and Balaram, P. (2001) Design of folded peptides. *Chem. Rev. 101*, 3131–3152.
24. Mathur, P., Ramakumar, S., and Chauhan, V. S. (2004) Peptide design using α,β-dehydro amino acids: From β-turns to helical hairpins. *Biopolymers 76*, 150–161.
25. Rudresh, Ramakumar, S., Ramagopal, U. A., Inai, Y., Goel, S., Sahal, D., and Chauhan, V. S. (2004) *De novo* design and characterization of a helical hairpin eicosapeptide: Emergence of an anion receptor in the linker region. *Structure 12*, 389–396.
26. Sudha, T. S., Vijayakumar, E. K., and Balaram, P. (1983) Circular dichroism studies of helical oligopeptides. Can 3(10) and α-helical conformations be chiroptically distinguished?. *Int. J. Pept. Protein Res. 22*, 464–468.
27. Formaggio, F., Crisma, M., Rossi, P., Scrimin, P., Kaptein, B., Broxterman, Q. B., Kamphuis, J., and Toniolo, C. (2000) The first water-soluble 3(10)-helical peptides. *Chemistry 6*, 4498–4504.
28. Yeaman, M. R., and Yount, N. Y. (2003) Mechanisms of antimicrobial peptide action and resistance. *Pharmacol. Rev. 55*, 27–55.
29. Raetz, C. R., and Whitfield, C. (2002) Lipopolysaccharide endotoxins. *Annu. Rev. Biochem. 71*, 635–700.
30. Nikaido, H. (2003) Molecular basis of bacterial outer membrane permeability revisited. *Microbiol. Mol. Biol. Rev. 67*, 593–656.
31. Hancock, R. E., Farmer, S. W., Li, Z. S., and Poole, K. (1991) Interaction of aminoglycosides with the outer membranes and purified lipopolysaccharide and OmpF porin of *Escherichia coli*. *Antimicrob. Agents Chemother. 35*, 1309–1314.
32. Boulos, L., Prevost, M., Barbeau, B., Coallier, J., and Desjardins, R. (1999) LIVE/DEAD BacLight: Application of a new rapid staining method for direct enumeration of viable and total bacteria in drinking water. *J. Microbiol. Methods 37*, 77–86.
33. Bracci, L., Falciani, C., Lelli, B., Lozzi, L., Runci, Y., Pini, A., De Montis, M. G., Tagliamonte, A., and Neri, P. (2003) Synthetic peptides in the form of dendrimers become resistant to protease activity. *J. Biol. Chem. 278*, 46590–46595.
34. Ulmschneider, M. B., and Sansom, M. S. (2001) Amino acid distributions in integral membrane protein structures. *Biochim. Biophys. Acta 1512*, 1–14.
35. Russell, A. D. (2002) Mechanisms of antimicrobial action of antiseptics and disinfectants: An increasingly important area of investigation. *J. Antimicrob. Chemother. 49*, 597–599.

36. Stratton, C. W. (2003) Dead bugs don't mutate: Susceptibility issues in the emergence of bacterial resistance. *Emerging Infect. Dis. 9*, 10–16.
37. Brogden, K. A., De Lucca, A. J., Bland, J., and Elliott, S. (1996) Isolation of an ovine pulmonary surfactant-associated anionic peptide bactericidal for *Pasteurella haemolytica*. *Proc. Natl. Acad. Sci. U. S.A. 93*, 412–416.
38. O'Farrell, P. Z., Goodman, H. M., and O'Farrell, P. H. (1977) High resolution two-dimensional electrophoresis of basic as well as acidic proteins. *Cell 12*, 1133–1141.
39. Svenson, J., Stensen, W., Brandsdal, B., Haug, B., Monrad, J., and Svendsen, J. (2008) Antimicrobial Peptides with Stability toward Tryptic Degradation. *Biochemistry 47* (12), 3777–3788.
40. Schafmeister, C. E., Gregory, J. P., and Verdine, G. L. (2000) An All-Hydrocarbon Cross-Linking System for Enhancing the Helicity and Metabolic Stability of Peptides. *J. Am. Chem. Soc. 122*, 5891–5892.
41. Weidenmaier, C., and Peschel, A. (2008) Teichoic acids and related cell-wall glycopolymers in Gram-positive physiology and host interactions. *Nat. Rev. Microbiol. 6*, 276–287.